HELSINGIN YLIOPISTO
HELSINGFORS UNIVERSITET
UNIVERSITY OF HELSINKI

RCD1 nuclear body dynamics and IDR2 phosphorylation in *Arabidopsis thaliana*

Shaimaa Roshdy Abdullah Reda

Master's thesis

Erasmus Mundus Master Program in Plant Breeding (emPLANT)

Master's Programme in Agricultural Sciences, Plant Breeding Module

The University of Helsinki, Department of Agricultural Sciences, May 2022

Abstract Form

Faculty	Department
Faculty of Agriculture and Forestry	Department of Agricultural Sciences
Author	Supervisor
Shaimaa Roshdy Abdullah Reda	Richard Gossens / richard.gossens@helsinki.fi

Title

RCD1 nuclear body dynamics and IDR2 phosphorylation in *Arabidopsis thaliana*

Subject

Plant molecular biology

Level	Month and year	Number of pages
M.Sc. Thesis	May 2022	37 + 9 Supplementary data

Abstract

Nuclear bodies (NB) have been studied for their importance of being one of the sites for gene regulation activities. RADICAL INDUCED CELL DEATH1 (RCD1) has proven to be a potential nuclear protein in *A.thaliana* that localizes to NB. It can interact with different transcription regulators responsible for many physiological functions. One of which is light signaling. Hence, it shares mutual functions with some phytochrome photoreceptors (PHYs), e.g., PHYB. It also contains intrinsically disordered regions (IDRs) that stabilize RCD1 protein upon phosphorylation. This study aims to examine the colocalization events of RCD1 that coexpressed with PHYB in full-length RCD1 complementation line and domain deletion lines, given the fact that both RCD1 and PHYB have previously shown mutual interaction with some of PHYTOCHROME INTERACTING FACTORS (PIFs). To achieve this aim, the colocalization of Venus-tagged RCD1 and Green fluorescent protein (GFP)-tagged PHYB using confocal Microscopy was performed. Another objective is to study the phosphorylation effect of one of the IDRs between WWE and PARP-like domain -IDR2- on RCD1 NB localization. Two phosphomutants -non-phosphorylatable and phosphomimetic- constructs were transiently and stably expressed in the *rcd1-4* background.

Furthermore, they were screened using Confocal Microscopy. We were able to see the colocalization events in 2 domain deletion lines, RCD1-ΔWWE-3xVenus and RCD1-ΔPARP-3xVenus. On the other hand, we could not see any colocalization in the RCD1-ΔRST-3xVenus, which indicates the importance of the RST domain in the colocalization. In addition, phosphorylation was found to affect the abundance of RCD1 protein in both transiently and stably expressed lines. Our study showed non-phosphorylatable forms of IDR2 having a higher abundance of RCD1 NB than the control line RCD1-3xVenus, whereas phosphomimetic IDR2 showed no signal. Collectively, Our experiments showed the effect of phosphorylation on RCD1 NB localization and the importance of the RST domain in the colocalization of RCD1 with PHYB.

Keywords

Nuclear bodies - RCD1– PHYs– *phyB*-5 – PIFs- Phosphorylation - IDR2- Non-phosphorylatable IDR – Phosphomimmitic IDR - Confocal Microscopy

Where deposited

Master's Programme in Agricultural Sciences, Department of Agricultural Sciences

Acknowledgements

I am limitlessly grateful to Allah, who gave me the power to start and continue this journey.

All my gratitude to my supervisor Richard Gossens, who provided me all the time with sincere advices and support along the way till the very last moments of submission. I am very thankful to Dr. Alexey Shapiguzov for being a wise mentor and offering this opportunity to me. Thanks to Prof. Jaakko Kangasjärvi for accepting me in his group, providing laboratory resources and opening up potential future chances. I am also thankful for my lab mates and lab technicians for their support and kind souls that I will never forget. I must also thanks Dr. Cezary Waszczak for sharing his practical tips in genotyping with me.

I have to thank my program coordinators in Beauvais and Helsinki, Alicia Ayerdi Gotor, Teemu Teeri, Minna Haapalainen, Aude Martin and Melanie Bedot who have always been in help with any matter I faced. As well as all my emPLANT family in all the cohorts. They proved to be a real family, not just friends, especially; Reham Nabil, Umama Hani, Danish Ahmed, Madan Kafle, and Paul Adunola.

I would like to say that nothing would have been done without my family specially and friends' support back home Egypt. They are the reason for who I am today. I would like to dedicate the achievements and success in this journey to them.

Thank you for reading.

The Author,

Shaimaa Reda

Talonpojantie 15 as 105

00790, Helsinki,

Finland

May 2022

Table of Contents

1. Introduction

Plants continuously receive signals from various environmental interactions that affect plant's physiology. This allows plants to send back a response on a structural and molecular level to cope with these signals. Vandereyken (2018) has reported that many interacting proteins, or so-called hub proteins, play an essential role in plant stress responses. RCD1, a potential hub nuclear protein, was discovered in *A.thaliana* via reactive oxygen species (ROS) sensitivity screen induced by ozone fumigation (Overmyer et al., 2000). The list of *rcd1* phenotypes has been growing steadily over many studies. RCD1 is a multidomain nuclear protein that comprises 589 amino acids. The domains of RCD1 are structured as follows, starting with the N-terminal nuclear localization sequence (NLS), followed by the WWE protein-protein interaction domain, a poly(ADP-ribose) polymerase-like (PARP-like) and C-terminus transcription factors interacting RCD1-SRO-TAF4 domain (RST). In addition to some interdomain regions, IDRs are believed to control the final conformation of the protein and its further nuclear compartmentalization (Leung, 2014; Vainonen et al., 2020) (**Figure 1**).

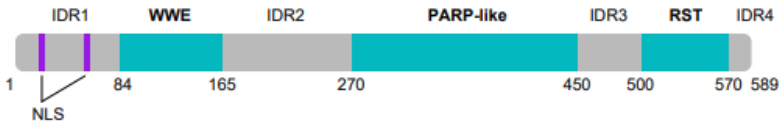

Figure 1. Illustrative picture of RCD1 conserved domains with representing numbers of residues for each domain. NLS, nuclear localization signal; PARP, Poly(ADP-ribose) polymerase; RST, RCD1-SRO-TAF4; IDR, Interensically disordered region. Reproduced from (Vainonen et al., 2020).

Many altered phenotypes were observed from the *rcd1* mutant line, such as early flowering, early leaf senescence, curl leaf-shaped and others (Hiltscher et al., 2014; Vainonen et al., 2012). Some phenotypes were studied as a response to deletion of the functional domain in RCD1 that interacts with transcription regulators. Hence these regulators facilitate phenotypic expression. In this shade, some findings drive our study, RCD1- interacting transcriptional regulators such as PIFs directly regulate light signaling via interacting with PHYs (Jaspers et al., 2009; van Buskirk et al., 2012). Another motor was that IDRs interestingly participate in RCD1 localization and stability (Vainonen et al., 2020).

This study used full-length RCD1 complementation and domain deletion lines to understand RCD1 and PHYB colocalization. Moreover, We studied the phosphorylation effect on IDR2 and further understood the RCD1 nuclear protein localization consequence.

2. Literature Review

2.1 Nuclear bodies and their types

Plants are well known for their diversity on the planet. The plant cell is the building block of the plants in which all the vital processes for plant health and development occur. One of the fundamentally essential compartments is the nucleus. The nucleus is a highly structured organelle that coordinates multiple developmental cell activities, such as cell division and gene expression. Many studies have found that the nucleus contains sub-compartments or NBs (Dundr & Misteli, 2010; Santos et al., 2020; Shaw & Brown, 2004; Staněk & Fox, 2017). Nuclear bodies were described as membraneless and microscopically visible structures. They vary in shape from spherical to irregular forms. NBs are generally dynamic, and their structure formation is affected by physiological, developmental and environmental cues (Staněk & Fox, 2017). Three theoretical models have explained the dynamics between NBs in the nucleoplasm (Dundr & Misteli, 2010). One of which is the stochastic model, which represents an assembly model of individual components to form NBs. This assembly happens through random interactions, not hierarchy towards the assembly.

On the other hand, there is an ordered assembly model, in which individual components have to follow sequential order to form NBs. Unlike the stochastic model, one or few pathways will form nuclear bodies in the ordered model. Seeding is the third assembly model in which RNA or proteins act as a seed for nuclear body assembly. The most studied NBs are the nucleoli, followed by Cajal bodies (CBs), nuclear speckles and paraspeckles (Kalinina et al., 2018a; Reddy et al., 2012b; Shaw & Brown, 2004) (**Figure 2**).

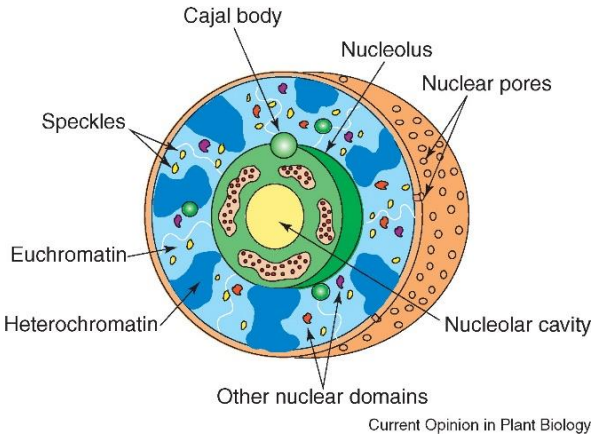

Figure 2. Graphical picture of nucleus structure: represents the main types of nuclear bodies and their distribution across the nucleus in the Euchromatin regions. Reproduced from (Shaw & Brown, 2004)

2.1.1 Nucleolus

The nucleolus is the largest and most prominent organelle in the eukaryotic nucleus. Nucleoli are well known for ribosomal subunits production and pre-mRNA processing (Kalinina et al., 2018). The size of the nucleoli varies from very small (>1 μm) in prokaryotes to 10 μm in Pea plants (Kalinina et al., 2018). Stępiński (2014) reviewed the ultrastructure of the nucleolus stating four main components. The fibrillar centre has fibrillarin as a critical protein for identifying nucleolus. Furthermore, other important sub nucleolar domains studied dense fibrillar components, granular components and nucleolar vacuoles. It has been revealed that the size and the numbers of the mentioned sub nucleolar components correlated with nucleolus transcriptional activity (Stępiński, 2014).

2.1.2 Cajal bodies

CBs were found to be close to the nucleolus in structure and function in Eukaryotic cells. In some cases, their existence is not vital to cell development and functionality (Mao et al., 2011). Their sizes ranged from 0.2 to 2 μm (Jády et al., 2000). They localize to nucleoli or are found across the nucleoplasm (Love et al., 2017). Cajal bodies are rich in diverse types of protein and RNA components. The most abundant ones are scaffolding proteins named Collin and U2B" spliceosomal protein. Green fluorescent tagged-Collin and U2B" were usually used in experiments to distinguish CBs from other NBs. (Love et al., 2017; Mao et al., 2011).

2.1.3 Nuclear Speckles

Nuclear speckles are known to store and assemble pre-mRNA components. Their shapes are highly affected by environmental and posttranscriptional activities like the high temperature, impaired transcriptional activity and phosphorylation. One of the well-studied nuclear speckles is the splicing regulators proteins and their rule in regulating many physiological plant processes like nutrients homeostasis and the hormone signalling affecting immune response (Bazin et al., 2018; Feng et al., 2020; Reddy et al., 2012). Splicing regulators (SRs) were found to be highly phosphorylated proteins which increasingly affects their activity (Reddy et al., 2012). It was noted that it was challenging to interpret whether Some SR protein families localize into speckles or partially (Reddy et al., 2012).

2.2 Nuclear bodies function

Various functions are interpreted from the previously discussed structures of different nuclear bodies. It has been thought that nuclear bodies can serve as a microenvironment. One of the most mentioned is that it is a place that brings proteins and RNAs together in a specific

concentration. They have also been described as a place where it interacts with other proteins for an ultimate function. Alternatively, they can be storage and/or modification sites for RNA and/or proteins that regulate gene expression (Mao et al., 2011). NBs could be further classified according to their biogenesis into two classes; activity-dependent and activity-independent. The former category is well represented by nucleolus, as it forms upon the transcriptional activity of the genes (Dundr & Misteli, 2010; Stępiński, 2014). Like Cajal bodies, nuclear speckles and other bodies, the latter have claimed to be present in specific sites in the nucleus; however, they are recruited to those sites to do their functions not necessarily produced in the same site like nucleolus (Dundr & Misteli, 2010). Kalinina (2018) has mentioned the sets of activities that have been studied in the nucleoli. Those activities include; Ribosome biogenesis, transcription regulation and silencing and, subsequently, their role in the development and disease/stress response. On the other hand, some bodies were formed and localized to the nucleus in response to light activities named photo bodies (van Buskirk et al., 2012).

2.3 Photobodies dynamics and function

Photobodies were defined by literature as a class of nuclear bodies that localized into the nucleus or subnuclear in response to light cues. Phytochromes (PHYs)-containing photobodies is the widely studied plant photoreceptor as they are most abundant in plant cells. PHYs have two main structure conformations that interconvert in response to light wavelength. One of which is the inactive form of so-called red light-absorbing phytochromes (Pr). Pr conformer activated by red light (λ_{max} = 660 nm) in consequence, it converts to its far-red light-absorbing phytochromes (Pfr) (λ_{max} = 730 nm) (Franklin & Quail, 2010; van Buskirk et al., 2012) see **Figure 3** PHYs exist as a dimer,e.g., PHYB + phytochromobilin known as apoprotein.

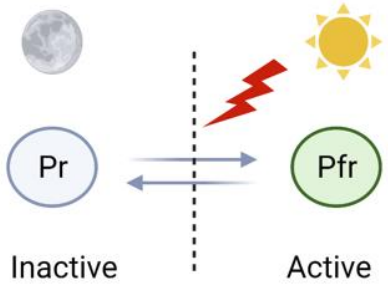

Figure 3. Graphical representation of red and far-red PHYS photoreceptors that interconvert in response to red light. This picture was created with Biorender.com.

2.3.1 PHYB localization and potential functions

Several studies using fluorescent proteins tagged PHYs have shown the localization of PHYs into the cytoplasm. The first report on nuclear and subnuclear localization of PHYB-GFP into small speckles was later discovered by Akira Nagatani (Yamaguchi et al., 1999). All PHYs (PHYA-E) in *A.thaliana* are localized to photobodies in light exposure. That interestingly later results in the nucleus translocation of PHYs (van Buskirk et al., 2012). PHYB has been tested to be the most stable type among PHYs, unlike PHYA, considered to be early photobodies that appear transiently and then degrade 1 hr after light exposure. In addition, the size of PHYB photobodies was correlated with exposure time to red light. It is reported by Chen (2003) that PHYB tends to localize in larger bodies with increasing red light intensity.

Nevertheless, the distinct function of NBs is to be revealed entirely. Photoreception is considered the main characteristic of PHYs. However, It has been hypothesized several models for the possibility of functions after photoactivation and photobodies formation, one of which was to be a place where whatever activity is coming from PHYs' activation is processed. Some other models believed that photobodies are potential sites for the degradation and ubiquitylation of critical transcriptional regulators. Alternatively, In another way, the possibility of being a place for TRs, and E3 ubiquitin ligases to localize into photobodies for further downstream responses. The last model was supported by evidence that one of the phytochrome interacting factor e.g., PIF3 colocalize with PHYA to photobodies before their degradation and PHYB (Jaspers et al., 2009). PIFs regulate light-dependent seed germination through their interactions with gibberellic acid and abscisic acid (Yang et al., 2020).

2.4 Important processes for NB Structure and development

2.4.1 Liquid-liquid phase separation (LLP)

From previously discussed paragraphs, we have found that cells can create microenvironments for certain vital activities, and those microenvironments were described variably depending on their types and activity. They are characterized by forming small condensates, speckles or memeranless-organelles (MLOs), commonly named nuclear bodies (Owen & Shewmaker, 2019). A hallmark of NBs that they are membraneless structures. The absence of membranes made NBs find a way to separate their components and activities from the rest of the cellular components. NB proteins tend to form protein aggregates, interact with other molecules and form what is described as liquid droplets. It is a process that resembles oiling out in vinaigrette, where vinegar and oil are separated.

Similarly, some proteins can separate from a solution in the cells, hence forming protein-rich droplets. Those droplets are aggregated with content-similar partners into compartments (Lafontaine et al., 2020; Owen & Shewmaker, 2019; Santos et al., 2020). This phenomenon was driven by physical interaction between two liquid phases that oppose the entropy-driven-mixing force of liquids (Hyman et al., 2014). This phenomenon has been studied mainly in animals and not too much in plants. As a comparative example, previously mentioned nucleolus proteins were found to be phase-separated into droplets. Santos (2020) reviewed the importance of disordered regions in phase-separating nucleolar proteins.

2.4.1.1 Intrinsically disordered regions (IDRs)

An exciting feature of LLPs proteins is having non-folded regions called IDRs. This region is composed of an amino acid chain lacking a protein tertiary structure. It gives flexibility to the proteins through a transient or reversible change of their conformation. It also can give accessibility to PTM hence allowing change of protein conformation and activity (Owen & Shewmaker, 2019). PTM acts as molecular switches that alter intermolecular interactions of MLOs and lead to different cellular responses. In this way, it is deduced that PTM could promote or suppress LLPS. Phosphorylation of IDRs has been shown to affect the LLP of NBs in animals (Owen & Shewmaker, 2019).

2.4.2 Phosphorylation

Protein phosphorylation, in general, and NB, in particular, play a crucial role in protein structure and function (Gökirmak et al., 2015; Li et al., 2020; Mach, 2016; Shapiguzov et al., 2019; Wirthmueller et al., 2018). Commonly phosphorylated amino acids are serine, threonine and tyrosine (Liu et al., 2020; Wirthmueller et al., 2018). The addition of phosphoryl group to amino acid residues allows changes in the total charge of protein molecules, consequently changing protein behaviour. It has been found that serine/threonine phosphorylation favour or disfavours protein liquid phase separation in animals (Owen & Shewmaker, 2019). Phosphorylation by some members of the PHOTOREGULATORY PROTEIN KINASES (PPKs) family was required for RCD1 stability in *A.thaliana* (Vainonen et al., 2020). PIFs were found to interact with PHYB and localize to photobodies before their degradation. (Franklin & Quail, 2010).

3. Objectives of the study

Our study focuses on revealing more about RCD1 as a potential plant nuclear body. Localization pattern is a theme of the study that was mastered with the help of Confocal Microscopy. PHYB photobodies were used in this study to track their behaviour together with RCD1 in a comparative way. In parallel, establishing phosphomutants of RCD1 were used to check the localization of RCD1 NBs affected by phosphorylation. Cloning systems were established to produce two phosphomutated forms of RCD1.

In brief, the study objectives are:

1- RCD1-3xVenus colocalization with *phyB-5*-GFP.

2- RCD1 nuclear body localization of the phosphomutated IDR2.

4. Materials and Methods

4.1 Plant Growth conditions

This study used full-length Venus-tagged RCD1, domain deletion lines (complemented into *rcd1-4*) and GFP- tagged *phyB*-5 as parental lines for the colocalization experiment. In addition, the *rcd1-4* line was used as background to introduce phosphomimetic and non-phosphorylatable forms of the RCD1-IDR2, described in **Table 1**. Those lines were planted in 7 cm^2 squared pots pre-prepared with a soil mixture of peat: vermiculite (1:1) provided by Agra-vermiculite, Kekkila Professional. The soil was watered using misting inside the pots before placing the seeds. Trays with individual pots were stratified in a +4 °C room in the dark for uniform germination. The trays were transferred to the growth room for two days with respective conditions of 220 μmol m^{-2} s^{-1} white fluorescent lamps, 12- hour photoperiod at 23/19 °C and 70/90% relative humidity (day/night).

Table 1. Resources table of Arabidopsis lines

Plant lines	Description	Reference
rcd1-4	Identifier:GK-229D11	NASC stock center
rcd1-4:**RCD1-3xVenus**	RCD1 gene fused with Venus and complemented in *rcd1-4*	Shapiguzov et al., 2019
rcd1-4:**RCD1ΔRST-3xVenus**	RCD1 has deleted RST was complemented in *rcd1-4* and fused with Venus	Shapiguzov et al., 2019
rcd1-4:**RCD1ΔWWE-3xVenus**	RCD1 has deleted WWE was complemented in *rcd1-4* and fused with Venus	Vainonen et al., 2020
rcd1-4:**RCD1ΔPARP-like-3xVenus**	RCD1 has deleted PARP was complemented in *rcd1-4* and fused with Venus	Vainonen et al., 2020
phyB**-5-GFP**	Single nucleotide polymorphism transgenic line of PHYB fused with the green fluorescent protein	Yamaguchi et al., 1999
rcd1**-4:RCD1$^{S/T}$IDR2^{A}-3xVenus**	Non-phosphorylable IDR2 Construct in (Table XX) was stably transformed in *rcd1-4*	This study
rcd1-4**:RCD1$^{S/T}$IDR2$^{D/E}$-3xVenus**	Non-phosphorylable IDR2 Construct in (Table XX) was stably transformed in *rcd1-4*	This study

4.2 Arabidopsis Seed Cleaning and Surface sterilization

Seeds from different lines were cleaned using sieves with an aperture width of 425 μm. Two diameter sizes were used, 200 mm and 150 mm, respectively. The sterilization process was performed in a laminar flow cabinet using 500 μl of 70% ethanol and 2% TritonX-100. After 10 minutes of gentle mixing, the washing solution was discarded. Following that, seeds were rinsed three times with 1 ml 99% ethanol, and a final wash with 500 μl 99% ethanol was done. Finally, seeds were collected in 1.5 ml sterile microcentrifuge tubes and then dried on a sterile filter paper for 2-5 minutes.

4.3 Crossing RCD1-3xVenus with *phyB*-5-GFP

Seven-day old seedlings of *rcd1-4*:RCD1-3xVenus, *phyB*-5-GFP plants and three domain deletion lines *rcd1-4:*RCD1ΔRST-3xVenus, *rcd1-4:*RCD1ΔWWE-3xVenus and *rcd1-4:*RCD1ΔPARP-like-3xVenus described in **Table 1** were transplanted into 8 cm^2 pots and were kept in respective conditions 220 µmol m^{-2} s^{-1} white fluorescent lamps, 12 hours photoperiod at 23/19 °C and 70/90% relative humidity (day/night). 4-5 weeks-old plants were ready for crossing as they formed 5 –6 inflorescence. A notice, *phyB*-5-GFP were early-flowering; they needed to be sown one week earlier than other lines. *phyB*-5-GFP plants were used as pollen donors. Open flowers and siliques were removed from the mother plants with inox Dumont no. 5 tweezer (Switzerland), open. Meristem and tiny buds were removed, leaving 2-3 buds with mid-size for emasculation. One flower bud was opened by pressing gently on the top of the bud to separate the petals and sepals. Then all immature anthers were removed. This process was done repeatedly with the rest of the buds. Emasculated plants were labelled with clear colour thread. The emasculated plants were let to rest in the growth room for 1-2 days for better crossing efficiency. *phyB*-5-GFP mature flowers were selected with a pair of forceps and then brushed gently on the stigma. Then plants were left in growth chambers to continue growing. After 15-20 days, long, thick and yellow siliques were harvested, and they were ready for sowing to the next generation. The crossings protocol adapted from Mittelsten Scheid, Gregor Mendel Institute of Molecular Plant Biology

4.4 DNA extraction and genotyping of F2 plants

F2 plants of crossings between RCD1-3x Venus lines and *phyB*-5-GFP were DNA-extracted using Mugur's 96 well format CTAB protocol. 96-tubes box was filled with 2-3 3mm steel beads and left on the ice. About two leaves per plant were collected and put directly on the tube box. Plant materials were frozen quickly by liquid nitrogen for 15-30 seconds. After that, Grinding was performed on tissues using a Mixer Mill once for 30 seconds. Then, samples were spun shortly in a centrifuge equipped with an adaptor to fit the tubes. Samples later were cooled down at +4 °C for 10-15 minutes. 400 µl of 2X CTAB extraction buffer (2% (w/v) Cetyltrimethyammoniumbromid (CTAB), 100 mM Tris-HCl pH 8.0, 20 mM EDTA pH 8.0, 1.4 M NaCl, 1% (w/v) Polyvinyl pyrrolidone (PVP 40) Mr 40000) were added. The mixture was vortexed briefly and incubated at 37 °C for 30-45 minutes. Samples were cooled down at room temperature for 10 minutes. Subsequently, 400 µl of chloroform was added, and a subsequent vortexing step at maximum rotation speed for 15 seconds. Then a centrifugation step at 4000 rpm for 15 minutes. After that, 300 µl of the aqueous phase was transferred to a

new 96-tubes plate. Then 400 µl of isopropanol was added with good mixing. Followed by centrifugation for 45 minutes at 400 rpm (precooled centrifuge +4 °C). After the supernatant was discarded, washing with 200 µl of 70% ethanol was done, followed by centrifugation for 15 minutes at 4000 rpm. Tubes later were air-dried at 37 °C for 1 hour. Then DNA samples were dissolved in MilliQ water and left at least for 16 hours at +4 °C for later use. Genotyping was performed to detect four alleles, RCD1-3xVenus, *phyB*-5-GFP, *rcd1-4* and *phyB*-5. PCR primers are provided in **Table 2,** and the PCR reaction conditions are shown in **Supplementary Tables 1, 2, 3, 4 and 5**. *rcd1-4* allele was checked by T-DNA specific primers represented by blue arrows in **Figure 4**. dCAPs primers were designed using the dCAPS finder 2.0 web-based tool (http://helix.wustl.edu/dcaps). Amplicons of RCD1-3xVenus, *phyB-5*-GFP, *rcd1-4* were migrated on 1.2 % agarose gel except *phyb-5* amplicons were detected using 3% agarose gel.

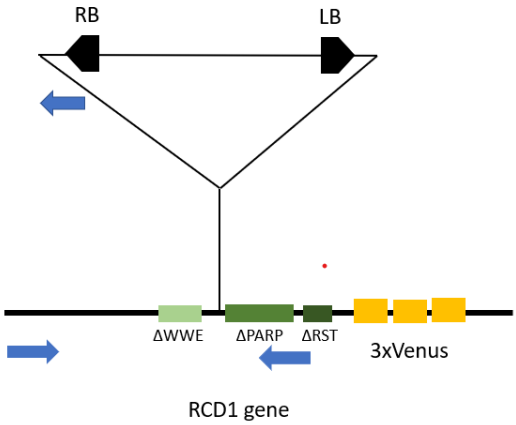

Figure 4. Illustrative model for RCD1gene and its rcd1-4 T-DNA insert

4.5 Plasmids Construction

The RCD1-3xVenus described in (Jaspers et al., 2009) was used. In the same way, non-phosphorylatable RCD1$^{S/T}$IDR2^{A}-x3Venus and phosphomimetic RCD1$^{S/T}$IDR2$^{D/E}$-3xVenus were constructed. Non-phosphorylatable and phosphomimetic IDR2 forms were synthesized by GenScript, Leiden, Netherlands. Both RCD1 backbone and phosphomutants were amplified by PCR using the primers in **Table 3**. and conditions in **Supplementary Tables 6, 7 and 8** and then DNA was precipitated by using 1/10th of the DNA volume of 3M sodium acetate and double the volume of Ethanol 70% was added then left overnight in -20 °C. The day after, DNA was tabletop-centrifuged at max speed for 10 minutes. It was followed by two washes of Ethanol 70% and centrifuged after each was for 2 minutes. The supernatant was discarded carefully, and DNA samples were allowed to air-drying or 42 °C heat block dying. DNA was dissolved in 30 µl MilliQ water, and DNA yield was estimated using NanoDrop^{TM} 2000.

After PCR gel electrophoresis check, purified products of backbone and inserts were used in golden gate cloning

Golden gate cloning aimed to replace the part of the gene with the wild type IDR2 region from the start of the coding sequence to the PARP-like domain with the mutated versions of IDR2. The Golden gate reaction components were described in **Supplementary Table 9** and illustrated graphically in **Figure 5**. Products of the golden gate were checked by restriction digestion **(Supplementary Table 11)** using *PstI* enzyme followed by gel electrophoresis migration using 0.8% agarose and 1xTAE buffer (40 mM Tris base, 20 mM Acetic acid, 1 mM EDTA pH 8.2 – 8.4) for 1 hour with 90-100 voltage.

Table 2. Primers for fluorophores, rcd1-4 T-DNA, and *phyB-5* dCAPs detection

Allele of detection	Forward primer	Reverse primer
RCD1-3XVenus	TGTACCAGTGCTGGATGTGG	ACCACTTTGTACAAGAAAGCTGGGT
phyB-5-GFP	ATTGTCAACTGCTAGTGGAAGTGG	GGTCTTGTAGTTGCCGTCGT
rcd1-4 (T-DNA)	CACAGTTGACTTTTTCTATCAAGGTT	ATAATAACGCTGCGGACATCTACATTTT
RCD1 (WT)	CACAGTTGACTTTTTCTATCAAGGTT	GCATCTTTATCAAGTACTTCGCT
phyB-5 (dCAPS)	GATAGTTTAGGCGATGCGGGGTATCC	TTTCTTTCGCAGTGTGAGATCGAAT

Table 3. Primers used for RCD1 backbone and insert amplification for golden gate

Primer name	**Forward**	**Reverse**
RCD1-IDR2	ATGGTCTCCGAAGCCAAGATCGTCAAG	ATGGTCTCCTCCCAACACCATAGATGGACT
pBm43GW	ATGGTCTCCGGGATCCATTTAACCGCTG	ATGGTCTCGCTTGACGATCTTGGCTTCC

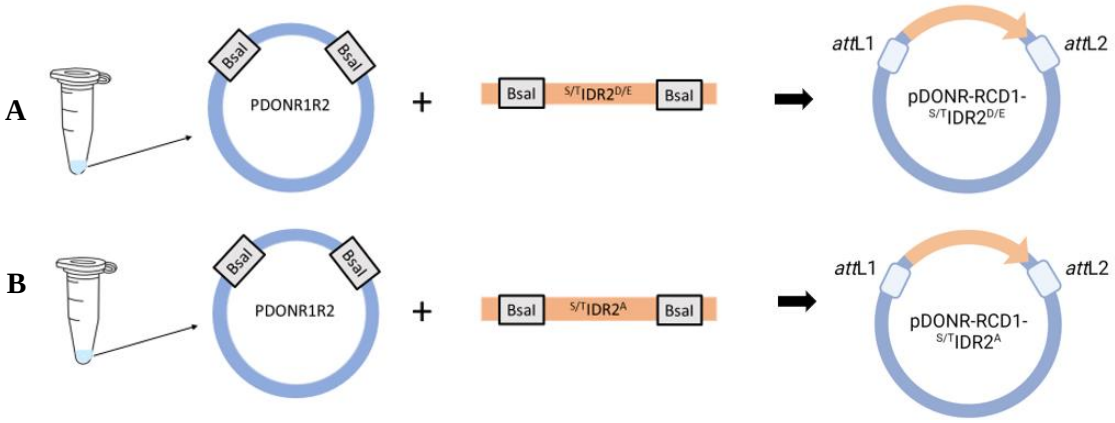

Figure 5. A scheme for golden gate cloning of IDR2 variants; pDONR1R2 having RCD1-IDR2 wild type, PCR fragments of RCD1-IDR2 phosphomutants; **A**: Phosphomemmtic form, **B**: non-phosphorylatable form. Furthermore, a final product of entry vectors having IDR2 phosphomutants and *att* sites.

Multisite Gateway cloning was performed using MultiSite GateWay® Pro LR Reaction Mixture provided by Invitrogen, US. Entry clones represent pDONR vectors with Ubquitin10 as a promoter, non-phosphorylatable and phosphomimetic mutated versions as CDS, and 3xVenus fluorescent protein merged with the OCS terminator. Entry clones were brought together in the pBm34GW destination vector mentioned in **Table 4,** illustrated graphically in **Figure 6**. The equimolar amount of each entry clone was used as ten fmol Entry: 20 fmol Destination as recommended. Reaction components were described in **Supplementary Table 10**. Gateway® LR Clonase™II Plus Enzyme Mix was incubated at 25 °C for 16 hours with respective amounts of vectors. Proteinase K was used to terminate the reaction by incubating it at 37°C for 10 minutes. The cloning mix was later Transformed into *Escherichia coli* Dh5α competent cells. Potential constructs were further checked by *PstI* enzymatic restriction digestions **(Supplementary Table 11 and Supplementary Figure 2**) and further by sequencing.

4.6 Heat shock transformation

Respective constructs were transformed by heat shock transformation using DH5α *E.coli* competent cells. This transformation was performed by thawing the competent cells on ice. After that, 5-7 µl of the cloning mixture were added to the competent cells, and then they were incubated on ice for 20 minutes. After that, competent cells are subjected to heat shock for 45 seconds at 42 °C. Subsequently, 1 ml of LB liquid medium was added to the transformation mix and incubation was done at 37 °C in the dark on the shaker. In Petri dishes, 20 ml LB agar medium was plated with suitable antibiotic (100 µg/1 µl) for selection **(Table 4)**. After 1 hour,

20 µl of the bacterial mix was added to the plates using sterile tips. The rest of the bacterial mix was centrifuged, and most of the medium was discarded. The left 50 µl of concentrated pellets were spread to another LB agar plate with a suitable antibiotic. A sterilized glass spreader was used to distribute the bacterial cells under aseptic conditions. After the cells were dried on the LB plates, They were kept at 37 °C for 16 hours. After the incubation, 6-12 colonies-to-screen were marked using a permanent marker. Sterile wooden toothpicks were used to pick the colonies and inoculate them into 5 ml of LB supplemented with suitable antibiotics for selection. The liquid cultures were incubated in a rotator/shaker at 37 °C for 16 hours.

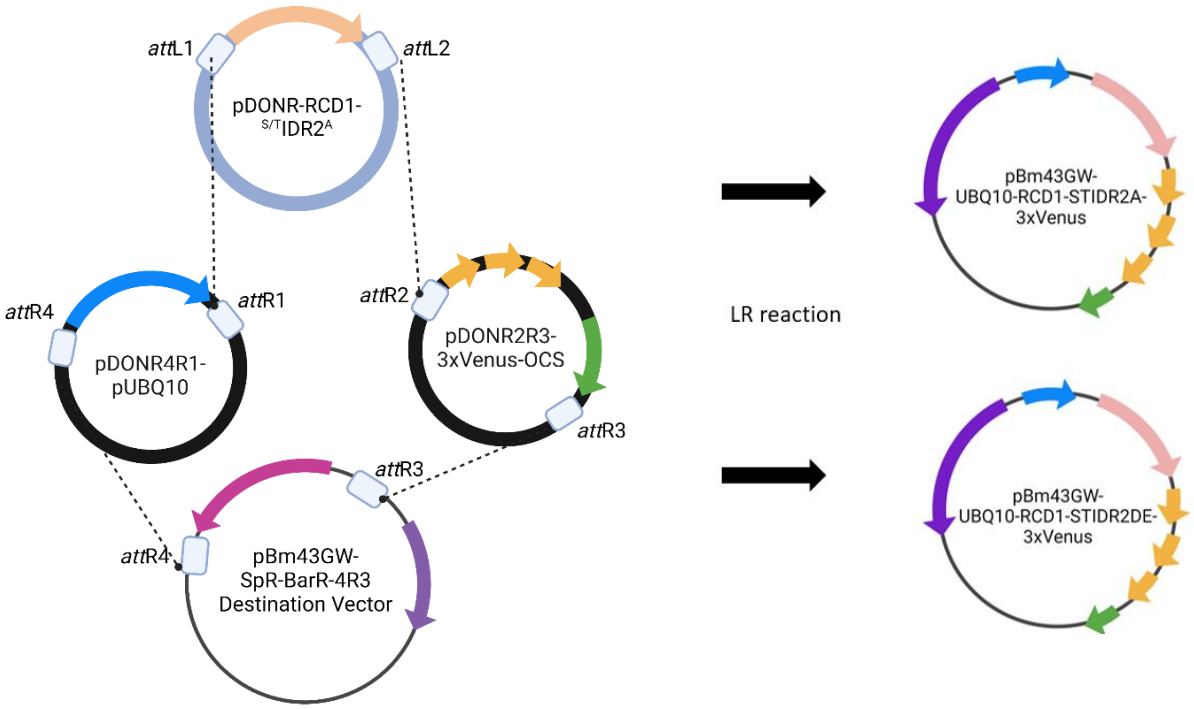

Figure 6. Schematic representation of multisite gateway cloning constructs used to build up the non-phosphorylatable and phosphomimetic forms of RCD1-IDR2-3xVenus via LR reaction. This figure was created with BioRender.com.

Table 4. Cloning vectors and constructs

Cloning vectors and constructs				
Abbreviation	**Description**	**Size**	**Resistance**	**Reference**
pBm43GW	Destination vector	9688 bp	Spectinomycin bacteria/Basta plants	Karimi et al., 2005
pDONR-pUB10	Constitutive Promoter	2811 bp	Zeocin	Siligato et al., 2015
pDONR-RCD1	RCD1 (CDS)	3840 bp	Zeocin	Jaspers et al., 2009
pDONR-3xVenus	Yellow fluorescent protein	6385 bp	Ampicillin	Jaspers et al., 2009
pDONR-RCD1-$^{S/T}$IDR2^{A}	Non-phosphorylatable form of RCD1-Entry Vector construct	3840 bp	Zeocin	This study
pDONR-RCD1-$^{S/T}$IDR2$^{D/E}$	Phosphomimetic form of RCD1-Entry Vector construct	3840 bp	Zeocin	This study
pBm43GW: UB10promoter-RCD1-$^{S/T}$IDR2^{A}- 3xVenus	Non-phosphorylatable form- Destination vector construct	13463 bp	Spectinomycin bacteria/Basta plants	This study
pBm43GW: UB10promoter-RCD1-$^{S/T}$IDR2$^{D/E}$-3xVenus	Phosphomimetic form-Destination vector construct	13463 bp	Spectinomycin bacteria/Basta plants	This study

4.7 Alkaline lysis miniprep

Alkaline lysis miniprep was performed based on Birnboim, H.C. (1983). Bacterial cells were harvested from overnight grown culture, then a centrifugation step was performed (> 12000 xg), and the media was discarded. Resuspension of harvested bacterial cells was done using sterilized solution *I* (0.1 mg/ml RNase, 25 mM Tris-HCl pH 8.0, 10 mM EDTA) precooled at + 4 °C. The lysis of bacterial cells was done using solution II (0.2 N NaOH, 1% SDS).

Tubes were inverted fast (not more than 5 minutes) and not vigorously shaken. Chilled neutralization solution *III* (potassium acetate: glacial acetic acid: MilliQ water 120: 23: 57 pH 5.5) was added to precipitate cell debris except plasmid left in the solution. Inverting the tube 4-6 times was done. After plasmid recovery by precipitation using an equal volume of isopropanol, a washing step with 70% ethanol was required to precipitate the plasmid and wash away the salts left bound to the DNA precipitate. Two rounds of washing with 1 ml 70% ethanol with centrifugation at >12000 xg for 10 minutes after each wash. DNA pellet was dissolved in 20-30 µl MilliQ water.

4.8 Selection and confirmation of successful clones

Constructs created by the golden gate cloning (pDONR-RCD1$^{S/T}$IDR2^{A} and pDONR-RCD1$^{S/T}$IDR2$^{D/E}$) **(Table 4)** were confirmed by restriction digestion with *pstI* and further confirmation by sequencing. Restriction digestions have been simulated *in silico* by Benchling.com. Sequence files were analyzed using multiple sequence alignment between pDONR-RCD1 wild type and IDR2 to verify the constructs. Both verified pDONR-$^{S/T}$IDR2 variants were further used in Multisite gateway cloning to get the expression constructs; pBm43GW: UBQ10 promoter-RCD1-$^{S/T}$IDR2^{A}-3xVenus and pBm43GW:UB10promoter-RCD1- $^{S/T}$IDR2$^{D/E}$-3xVenus. Those expression constructs were transformed to *Agrobacterium tumefaciens* GV3101 pMP90 strain for transient and stable line *A.thaliana* transformation.

4.9 FAST Agro-mediated seedling Transient Transformation (FAST)

All the following steps were performed under aseptic conditions. On day one, *rcd1-4* were surface-sterilized and sown on 0.5 X (2.2 g MS, 0.3 g MES, 3 g Gelzan, 5 M KOH, up to 1 Litre MilliQ) with 1% w/v sucrose. Then, seeds were stratified at +4 °C for > 24 hours. On day two, Seeds were moved to long-day growth chambers 16: 8 hours (light: dark) at 20-22 °C for four days. On day five, A preparation of *A.tumefaciens* either from a plate or glycerol stock with the respective constructs having the following genes RCD1-3xVenus, RCD1-$^{S/T}$IDR2^{A}-3xVenus, RCD1-$^{S/T}$IDR2$^{D/E}$-3xVenus. With a sterilized wooden pick, a colony or a scoop of cells was picked and inoculated in 50 ml LB Broth supplemented with Rifampicin(Rif) 50 mg/µl, Spectinomycin(Spec) 100 mg/µl and Gentamycin(Gent) 100 mg/µl. Liquid cultures were left to grow for 18-24 hours at 28 °C on a shaker to reach OD_{600} >1.5. On day 6, OD_{600} was checked on the 1/10th dilution. Cells were spun at room temperature for 10 minutes. The following formula was used to calculate the amount of both washing solution and cocultivation medium to resuspend the pellets with:

X(washing/cocultivation solution) in ml= OD_{OBS}*Dilution factor*Volume/OD_{Final}

(e.g. Final OD= 2.5)

After the washing and cocultivation solutions were calculated, 100 µM of acetosyringone was added before the washing step. Cells were further resuspended in an X ml washing solution. After that, cells were spun again for 10 minutes. After discarding the washing solution, cells were resuspended with X ml of cocultivation medium with pre-addition of 100 µM of acetosyringone and 0.005% (v/v) Silwet L-77. Cells were incubated at room temperature for 2 hours. 10 seedlings (4 days-old) per plate/ construct were soaked in 1-3 ml of Agrobacterium + cocultivation solution. Cotyledons were fully submerged. Seedlings were incubated with a cocultivation mixture for 15-20 minutes. Five to six dry-sterilized circled cut filter paper (suits petri dish inner diameter) were layered in a petri dish. The filter papers stack was soaked with approximately 10 ml of cocultivation medium. In the end, seedlings were transferred to the filter papers stack and incubated for approximately 40 hours in the dark at room temperature. Afterwards, seedlings are moved to light and ready to be screened with confocal laser microscopy for Venus signals.

4.10 Floral pipetting for stable transformation

$RCD1^{S/T}IDR2^{A}$-3xVenus and $RCD1^{S/T}IDR2^{D/E}$-3xVenus were transformed to *A.tumefaciens* GV3101 pMP90 strain, 100 µl aliquot of competent cells were thawed on ice for 20 minutes. 500-1000 ng/µl of constructs were added. Cells were incubated on ice for 20 minutes with respective plasmids. The tubes were directly immersed in liquid nitrogen for 10 seconds then the tubes were picked and thawed by hand. 1 ml sterilized LB broth was added and incubated for 4 hours at 28 °C. Cells were spread on LB agar plates with Rifampicin (50 mg/µl), Gentamicin (100 mg/µl) and spectinomycin (100 mg/µl). The streaking step is to be done after pelleting the cells leaving 50-80 µl of media for spreading purposes. Under sterilized conditions, the plates were allowed to dry and incubated for 3-4 days. A single colony was picked from the 4-days old culture plate to inoculate 5 ml for 16 hours. Liquid culture with previously mentioned antibiotic selections at 28 °C for 16 hr. The next day, the cells were pelleted in 2 ml microcentrifuge tubes at 2000 rpm for 2 minutes. After discarding the supernatant, 5% sucrose w/v was added to the pellet as a transformation buffer. 0.02% v/v Silwet L-77 was added just before the transformation event. Floral buds were inoculated with 5-10 µl of *A.tumefaciens* transformation solution. Plants were kept in the dark for 24 hours. Then plants were exposed to light and other growth conditions as described above.

4.11 Phosphinothricin selection for T1 plants

Two months-old potentially transformed *A.thaliana* plants with respective constructs RCD1$^{S/T}$IDR2^{A}-3xVenus and RCD1$^{S/T}$IDR2$^{D/E}$-3xVenus **(Table 1)** were harvested and cleaned. Two sets of trays having 28 square pots with 7 cm^2 were watered, and seeds were spread equally. After 1-2 days of cold stratification, plants were moved to a short day growth room. Five-day-old plants were sprayed with phosphinothricin, commercially known as Basta, with a concentration of 120 mg/L. A second dose of phosphinothricin was given to 8 days-old plants. In one month, plants were ready to be screened via confocal Microscopy for Venus signal and then brought to the long-day growth room for T2 seed production.

4.12 Leaf discs preparation

From 4 weeks old F1 RCD1-3xVenus crosses with *phyB-5*-GFP plants, leaf discs samples were collected. One leaf disc was taken from each plant and treated with Milli-Q water + 0.05% tween-20 using a thin metal tube. For the T1 of RCD1-IDR2 phosphomutated variants, no treatment was done on them. Afterwards, to enhance the Venus signal, Leaf discs were loaded on a 96-well plate and kept at +4 °C and covered with aluminium foil (dark condition) for 16 hours. The following day, plants were ready to be screened for Venus and GFP signals in dark conditions through confocal laser microscopy.

4.13 Confocal Microscopy and imaging

Either stable Arabidopsis lines or transiently expressed plants were screened for RCD1 NB localization using confocal microscopy platform STELLARIS 8, manufacturer Leica Microsystems Wetzlar, Germany. This Microscopy was integrated with a hybrid detector (HyD^{TM}) and white light laser (WLL). Leica platform software (LASX) was used to adjust screening parameters. 528-600 nm YFP signal was harvested by using 518 nm excitation. For GFP, excitation was adjusted to 495 nm and harvested at 500-525 nm. Chloroplasts autofluorescence was detected at 650-750 nm with excitation of 495 nm from WLL (Kodama, 2016). In addition, the conventional photomultiplier (PMT) was used to detect the bright field images.

4.14 Image analysis

Images taken by the confocal microscopy camera were analyzed and processed using ImageJ software. To eliminate the background noise of the photo, Gaussian blur with radius two was applied. The imaging output was a stack of pictures representing four channels through which Venus and GFP signals were detected. In addition, the stack of photos was processed to be

merged into one image that projects the max intensity. Moreover, this was done by splitting the stack and merging channel functions. Image J Macro script was developed to analyze a group of images simultaneously. For analyzing pictures of RCD1-3xVenus colocalization with *phyB*-5-GFP, **Supplementary Code 1** was used. For RCD1-IDR2-3xVenus non-phosphorylatable and phosphomimetic detection, the script was used only for the Venus signal (**Supplementary Code 2.**). Comments in the script started with a double slash and green coloured indicating the function description.

5. Results

5.1 Genotyping

Two approaches were considered to study RCD1-3xVenus and *phyB-5*-GFP patterns and colocalization—one of which confocal microscopy screening of F1 and F2 plants. In parallel, genotyping of F2 plants has been performed to confirm the genotypes that show signals coming from both protein fluorophores. Parental lines were chosen where RCD1 domain deletion lines were pollen acceptors, and the *phyB*-5-GFP line was a pollen donor. *phyB*-5-GFP lines were planted one week earlier than other lines as they were early flowering. After F2 development, DNA was extracted using CTAB chloroform-based method from 5 weeks old plants. Genotyping was designed to detect four alleles in the F2; RCD1-3xVenus, *phyB*-5-GFP, *rcd1-4* and *phyB-5*. Those alleles were genotyped in four plant lines; RCD1-3xVenus, RCD1ΔWWE-3xVenus, RCD1ΔPARP-3xVenus and RCD1ΔRST-3xVenus with primers described in **(Table 2)**. PCR protocols were designed *in silico* with respective conditions **(Supplementary Tables 1, 2, 3, 4 and 5)**. Detected molecular weights matched the expected weights. In the RCD1-3xVenus crossed line, Venus was detected on 917 bp and GFP on 406 bp, examples of fluorophores detected in plant numbers 2 and 3 **(Figure 7)**. However, the expected molecular weights of RCD1 domain deletion crossed lines vary compared to the RCD1-3xVenus cross. RCD1ΔWWE-3xVenus cross exhibited the same molecular weight of RCD1-3xVenus cross as the primers amplified mid of PARP domain, RST domain and the start of Venus sequence (comprises 917 bp). Plant samples number 3 and 4 exhibit positivity to both fluorophores. In the RCD1ΔPARP-3xVenus cross, RCD1-3xVenus fluorophore was detected on 500 bp molecular weight, and plant sample number 2 showed detection in the two fluorophores. RCD1ΔRST-3xVenus cross was shown on a size of 550 base pair with the positivity of the two fluorophores detection in sample number 3 **(Figure 7)**. The genotypes that showed positivity to RCD1-3xVenus and *phyB-5*-GFP fluorophores were further detected for the *rcd1-4* and *phyB-5*. The *rcd1-4* genotyping is described in **Figure 8,** where sample number 1 showed homozygous wild type RCD1, sample number 3 showed heterozygous alleles RCD1 wild type and *rcd1-4*. sample number 5 showed homozygous to *rcd1-4*. *phyB-5* mutant dCAPs-based genotyping was not detectable, and It needed further optimization. The expected results of *phyB*-5 designed *in silico* and the obtained ones showed in **Figure 9**.

In conclusion, several descendants from the crosses were positive for both RCD1-3xVenus and *phyB*-5-GFP. Up to 17 plants were positive for both fluorophores out of 50 per crossed line. One to five fluorophores-positive individuals showed homozygosity for the *rcd1-4* allele. Individuals that exhibit bands in both fluorophores and homozygous for *rcd1-4* were picked for further confocal microscopy signal detection.

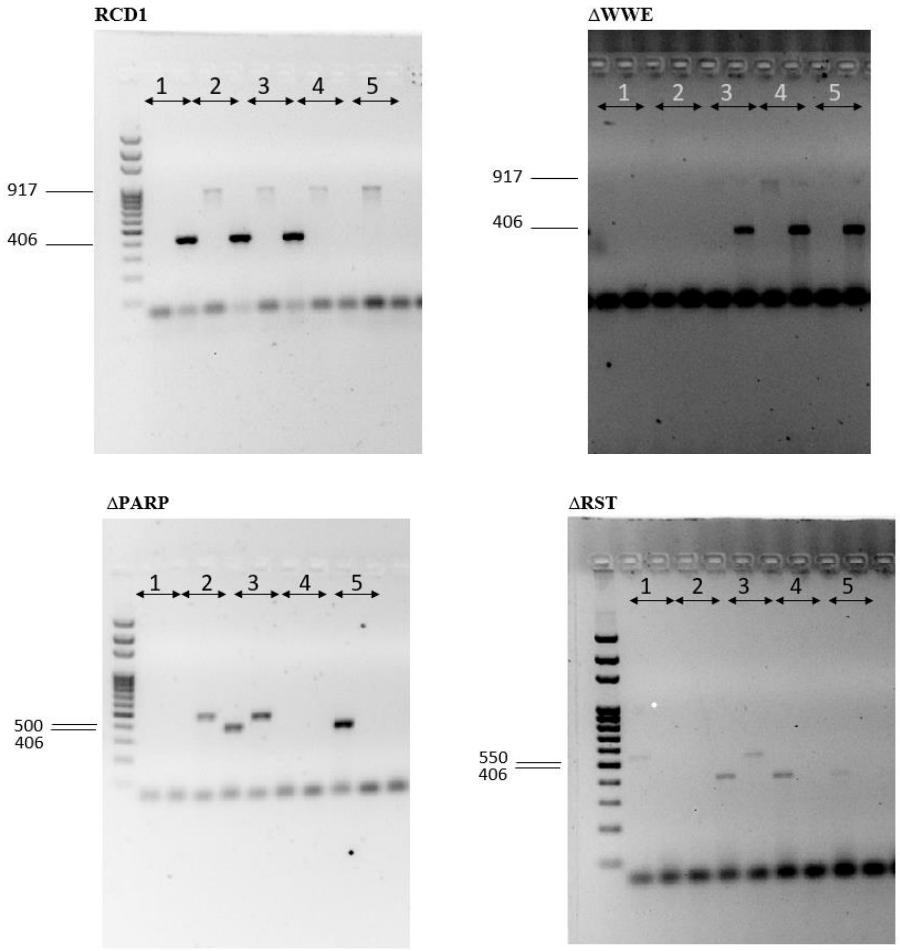

Figure 7. Gel electrophoresis images for RCD1-3xVenus and *phyB*-5-GFP detection in 4 genotypes; RCD1wild type, RCD1ΔWWE, RCD1ΔPARP, RCD1ΔRST with respective molecular weights expected for each genotype. RCD1-3xVenus was detected on Molecular weights of 917, 917, 500, and 550 with lines order. And, *phyB*-5-GFP bands were detected on 406, assigned molecular weights in base pair. Arrowed lines represent one plant sample detected for both fluorophores. Straight lines represent the bands shown on the gel on the expected molecular weight.

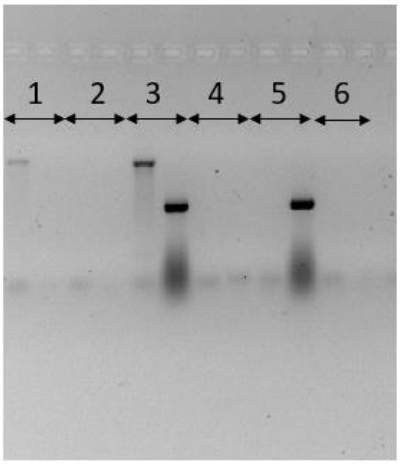

Figure 8. An example of a gel electrophoresis image for *rcd1-4* genotyping results. Samples are arranged from 1 to 6. Every two lanes represent one individual (shown by the two-arrowed line). Plant number 1 shows a homozygous allele for the RCD1 wild type. Plant number 3 shows heterozygous alleles for RCD1 and *rcd1-4*, and plant number 5 represents the homozygous allele for *rcd1-4*.

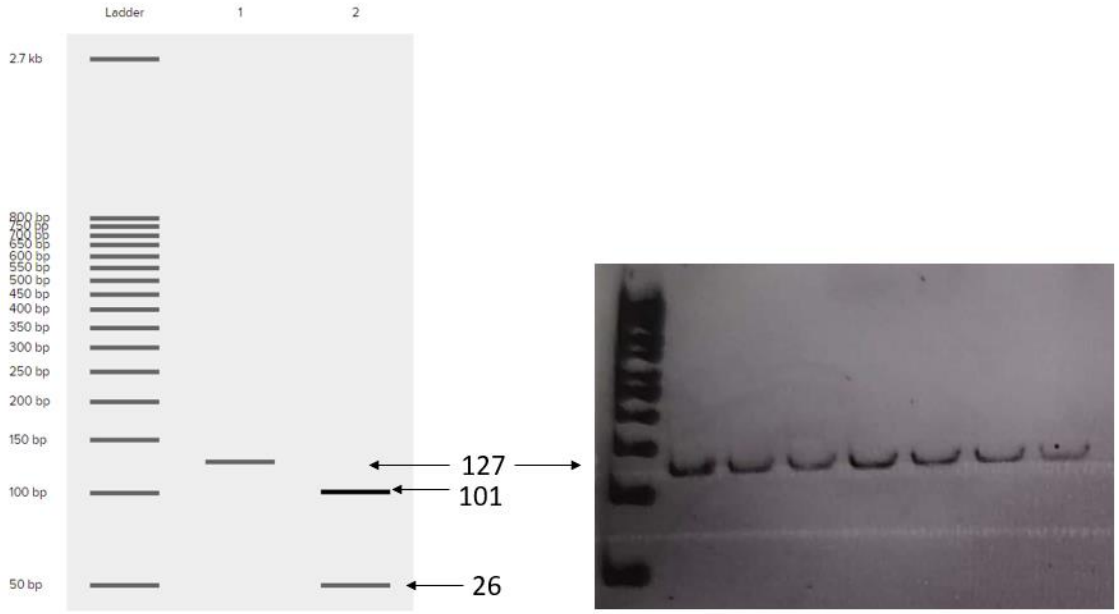

Figure 9. Example of EcoRI digestion of RCD1 genotype having *phy*B-5 allele. Left side picture: represents *in silico* digestion; Sample number 1 represents the wild type allele having 127 bp, and sample number 2 represents *phyB*-5 is having 101 and 26 bp. On the right side picture, EcoRI digestion that shows wild type *phyB*-5

5.2 RCD1 and PHYB colocalization pattern

To study the localization of RCD1-3xVenus to NB, RCD1-3xVenus was coexpressed with *phyB*-5-GFP. Crossings between full length RCD1-3xVenus and domain deletion lines with the *phyB*-5-GFP line have been performed. In 1 or 2 weeks after the crossings, siliques of the potential plants were harvested and grown to the F1 generation. 1-month-old F1 crossed plants were used in confocal microscopy screening. Using Confocal Microscopy, we adjusted the excitation and detection parameters to reasonably detect each fluorophore. However, It was challenging to clearly distinguish both fluorophores in GFP and Venus channels. As both

excitation and emission ranges of the two fluorophores were highly similar. Control lines used in this experiment were *phyB*-5-GFP and RCD1ΔPARP-3xVenus since RCD1ΔPARP-3xVenus had higher Venus intensity than RCD1-3xVenus full length. To ensure that certain fluorophore was detected, most signal intensities came through the detected channel and dimmed in the other channel **(Figure 10)**.

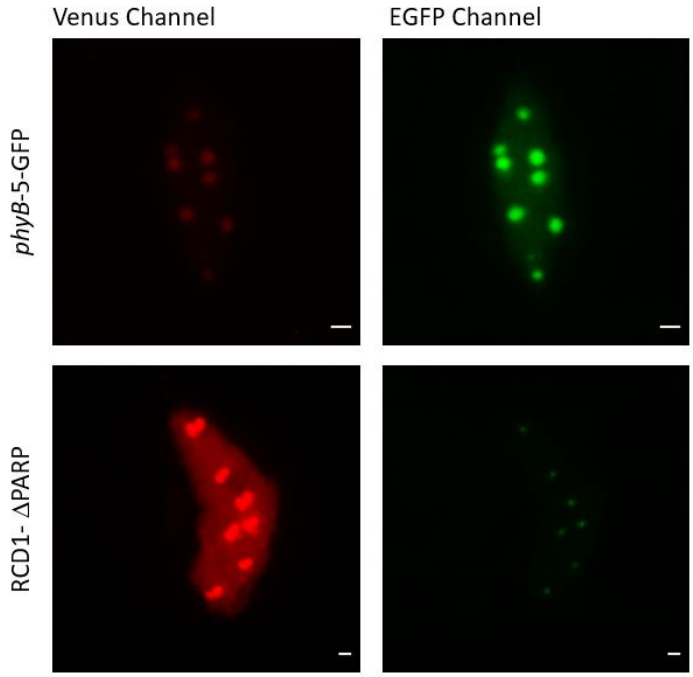

Figure 10. Confocal microscopy images for *phyB*-5-GFP and RCD1-ΔPARP as controls for GFP and Venus signals

All RCD1-3xVenus and *phyB*-5-GFP were observed to be localized to NB and nucleoplasm. RCD1-3xVenus crossed lines with phy*B*-5-GFP showed few small and mid-size RCD1 bodies. There was almost no clear colocalization **(Figure 11)**. On the contrary, The domain deletion line showed different patterns of colocalization. RCD1ΔWWE-3xVenus **(Figure 11)** showed various RCD1 body sizes; a few large ones and many small ones. The large ones only colocalized together with the spherical shaped PHYB. RCD1ΔPARP-3xVenus showed large nuclear bodies localized fully to PHYB compared to other lines **(Figure 11)**.

Interestingly, RCD1ΔRST-3xVenus was barely showing any colocalization. This result suggests that the presence of the RST domain is essential for RCD1-3xVenus colocalization with *phyB*-5-GFP. This observation was supported by the fact that the RST domain mediates the interaction with transcription factors like PIFs; PIFs were also found to interact with PHYB. A function of image calculation in ImageJ software was used to analyze those results further. An image calculator function was used to divide the two images of Venus and GFP channels.

In other words, dividing all the pixels present in the Venus channel by the pixels in the GFP channel. In the right section of ratio Venus/GFP **(Figure 11)**, colour references of the pseudo images and their values were attached in the ratio section legend. Applying this function, we further confirmed the previous observations on the colocalization events between RCD1 full length and domain deleted lines with PHYB, especially a clear colocalization in RCD1ΔWWE-3xVenus and RCD1ΔPARP-3xVenus were observed. And almost none in RCD1ΔRST-3xVenus.

From these results, RCD1-3xVenus and *phyB*-5-GFP localization to NB was emphasized. Colocalization of RCD1-3xVenus and *phyB*-5-GFP showed partially in RCD1ΔWWE-3xVenus and fully in RCD1ΔPARP-3xVenus with almost none in RCD1ΔRST-3xVenus which may potentially suggest the RST domain is vital for protein colocalization with *phyB*-5-GFP as it is the responsible domain for transcription regulators' interactions. However, these results needed further analysis and confirmation through F2 and F3 generation. With refined confocal imaging parameters.

5.3 Phosphorylation effect on RCD1 subcellular localization

To investigate the IDR2 phosphorylation effect on RCD1 NB localization *in vivo*, two versions of phosphomutants IDR2 region in RCD1 described in (Vainonen et al., 2020) were used. Those IDR2 phosphomutants comprise the non-phosphorylatable and phosphomimetic forms of RCD1. Plasmids having the RCD1-IDR2 wild type were replaced by golden gate cloning with PCR product of non-phosphorylatable $^{S/T}IDR2^{A}$ and phosphomimetic $^{S/T}IDR2^{D/E}$. Then multisite gateway cloning was used to build up the expression construct by bringing the UBQ10 promoter, 3xVenus and terminator in the pBm43GW destination vector. Both Entry intermediate clones **(Supplementary Figure 1)** and expression constructs **(Supplementary Figure 2)** were further checked by digestion with the *pstI* enzyme, which gave a pattern to distinguish between RCD1 wild type and phosphomutants. As illustrated in the experimental workflow **(Figure 12)**, Constructs were further transformed to *E.coli* and then into *A.tumefaciens* to proceed for either stable or transient line development. *rcd1-4* plants were used as a background to transform RCD1-3xVenus wild type, RCD1- $^{S/T}IDR2^{D/E}$-3xVenus and RCD1- $^{S/T}IDR2^{A}$-3xVenus. We have generated transiently expressed phosphomutated RCD1 plant population and stable lines. The transient transformation was a time-efficient assay to screen the localization pattern. Confocal pictures were taken from freshly prepared leaf discs.

Venus signal coming from transiently expressed lines seemed higher in *rcd1-4*:RCD1$^{S/T}$IDR2^{A}-3xVenus than *rcd1-4*:RCD1-3xVenus wild type. In contrast, *rcd1-4*:RCD1$^{S/T}$IDR2$^{D/E}$-3xVenus exhibit no signal **(Figure 13A**).

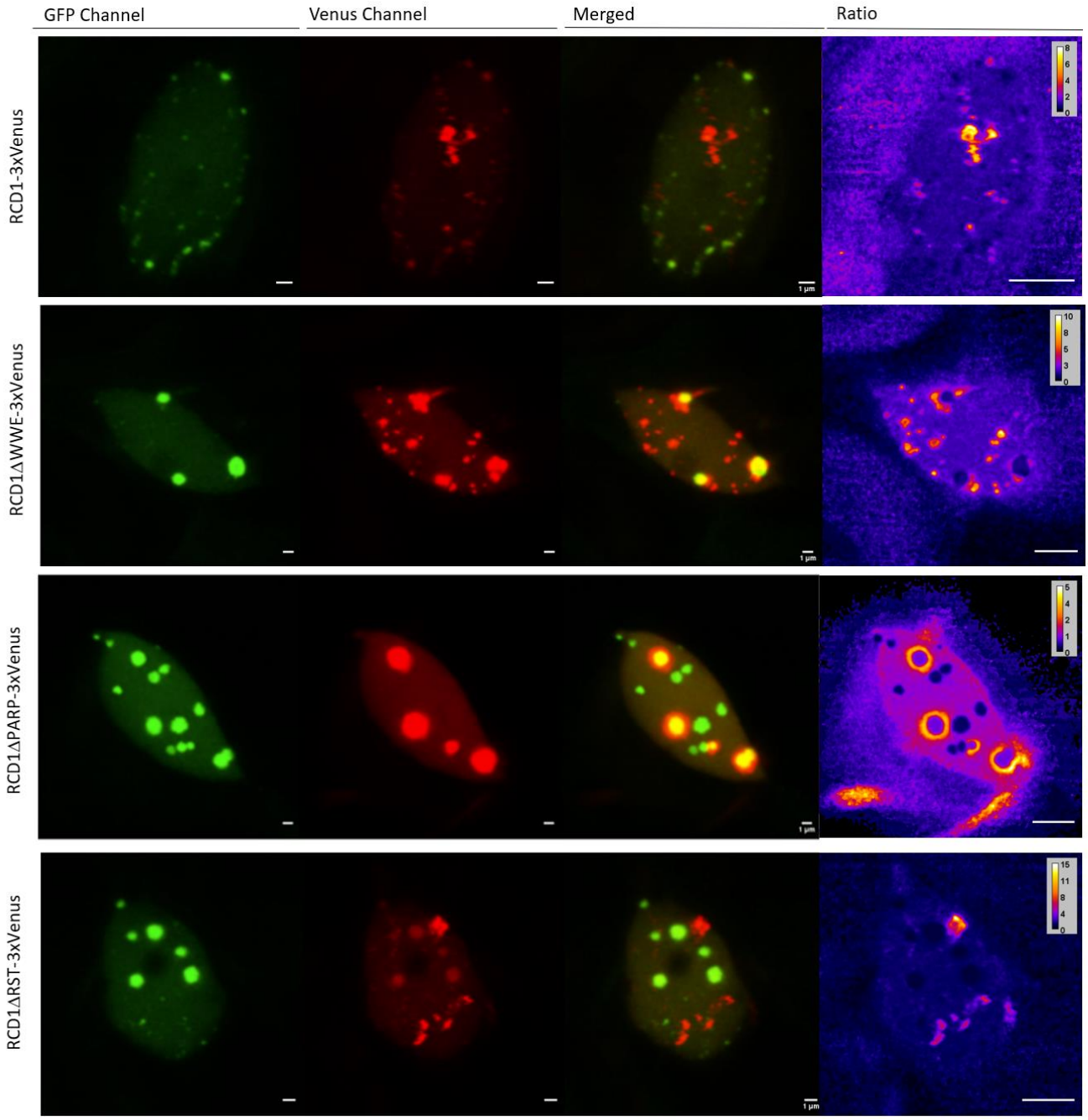

Figure 11. Confocal microscopy images for F1 generation of RCD1-3xVenus, RCD1ΔWWE-3xVenus, RCD1ΔPARP-3xVenus, RCD1ΔRST-3xVenus crossed with *phyB*-5-GFP. The channels used to detect the signal of fluorophores were GFP, Venus, merged channel and a pseudo image of Venus/GFP ratio. (Scale bar adjusted to 1 μm to all channels, scale bar in Ratio = 4 μm)

Moreover, T1 phosphinothricin-resistant stably expressed lines showed a good abundance of non-phosphorylatable *rcd1*-4: RCD1$^{S/T}$IDR2^{A}-3xVenus. Unlike non phosphorylatable RCD1, phosphomimetic *rcd1*-4: RCD1$^{S/T}$IDR2$^{D/E}$-3xVenus showed no signal **(Figure 13B)**. The RCD1-3xVenus stable control line was not shown in this experiment. However, It would be interesting to include the control in future trials. Those results suggest that the mutations on 15 phosphosites residues of IDR2 affect the localization and abundance of RCD1 nuclear bodies. Quantification of protein abundancy and immunoblotting in both variants to be performed for further validation.

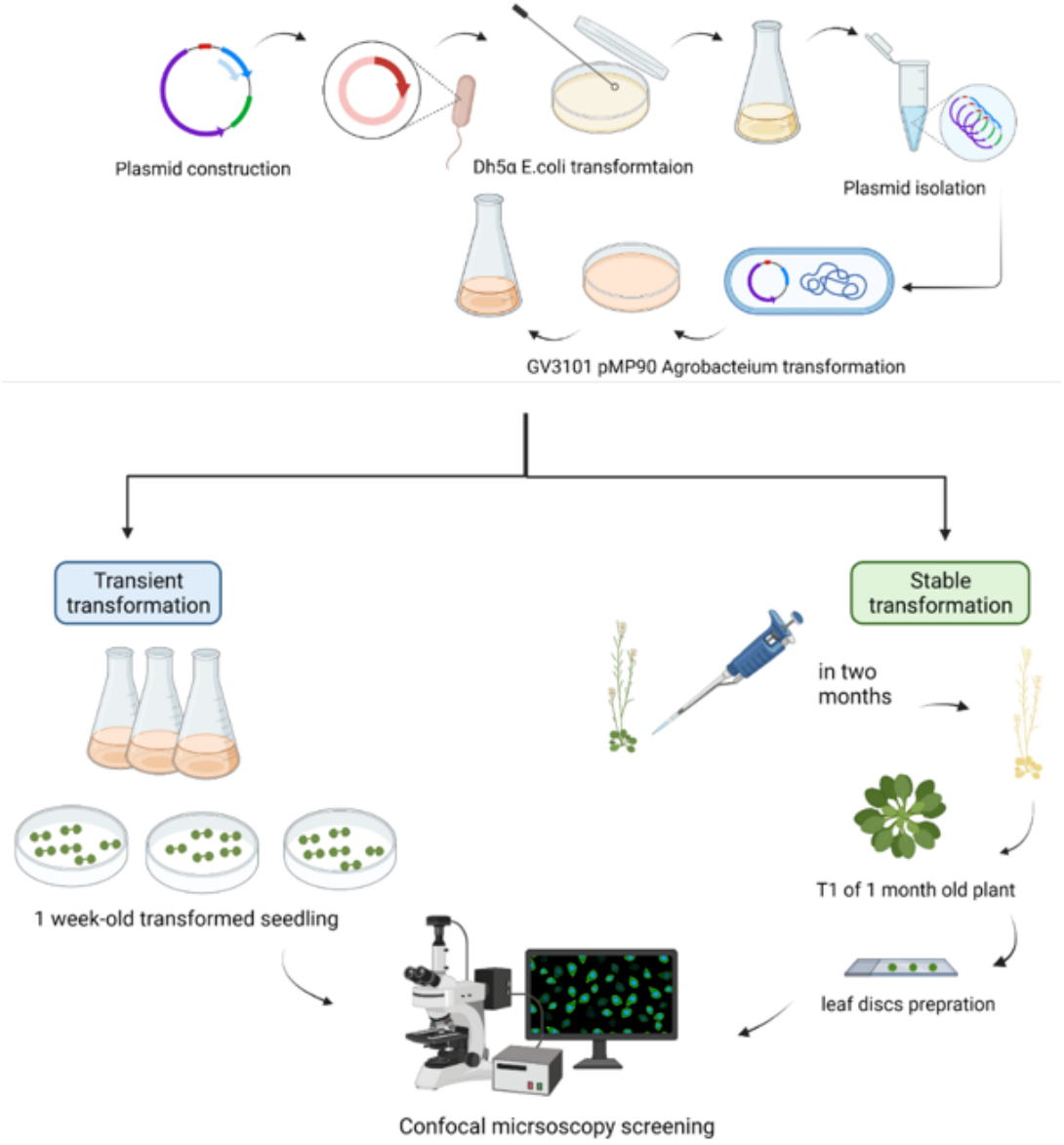

Figure 12. Experimental workflow of IDR2 phosphomutants development.

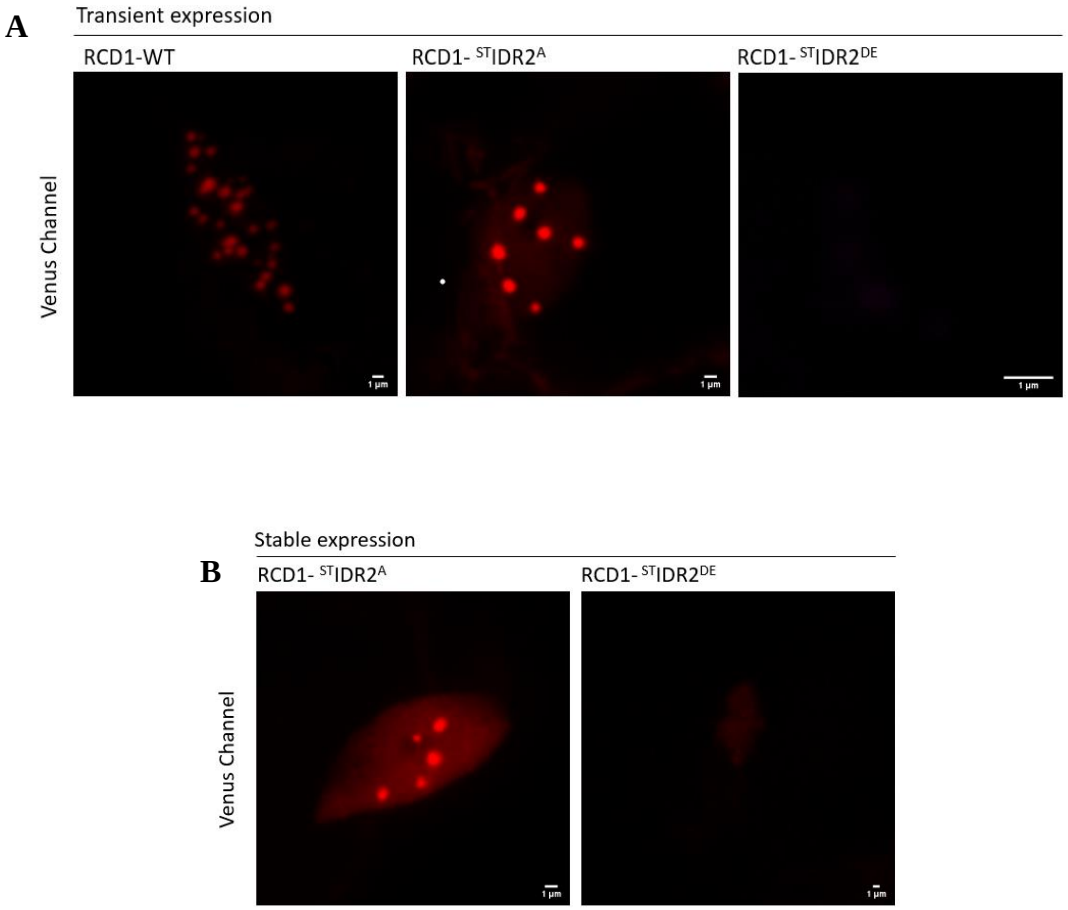

Figure 13. Confocal microscopy images of RCD1 NB localization. **A**: Venus signal detected in 3 transiently expressed RCD1 forms; 1 wild type and 2 of phosphomutated plants population. The transient assay was replicated three times to ensure consistency. Results of one replicate are shown. **B**: Venus signal detected in 2 stable expressed lines. The lines used in the assay; Non-phosphorylatable RCD1-$^{S/T}$IDR2^{A}-3xVenus and phosphomimetic RCD1-$^{S/T}$IDR2$^{D/E}$-3xVenus on the right side (scale bar adjusted to 1 µm).

6. Discussion

Plants are regularly experiencing adverse stress conditions, either biotic or abiotic. For the plants to cope with these stressors, They provoke physiological and biochemical changes (Zhang et al., 2022). With the help of hub proteins, plants can adjust their responses through hub protein interactions with different transcription factors. (Vandereyken et al., 2018; Jespersen & Barbar, 2020). RCD1 protein was recognized as a potential hub protein in many studies (Jaspers et al., 2009; Shapiguzov et al., 2019; Vainonen et al., 2012). It is well known for its pleiotropic phenotypes due to altering the gene activities of its interactors (Jaspers et al., 2009, 2010; Overmyer, Tuominen, Kettunen, Betz, Langebartels, Sandermann, et al., 2000). IDRs were found to help RCD1 interact with various transcription regulators by altering the conformation, affecting further binding (Owen & Shewmaker, 2019; Vainonen et al., 2020). PIFs were found to be interacting with RCD1 through its RST domain, suggesting a possible function of RCD1 towards light response (Jaspers et al., 2009).

6.1 RCD1ΔRST-3xVenus colocalizes with PHYB-GFP

RCD1, as a nuclear protein, was found to be localized to NB in both transiently and stably expressed *A.thaliana* (Vainonen et al., 2020). Our results emphasized and further validated this finding. PHYB bodies were observed to have distinct and constant shapes in both RCD1 wild type and domain deletion lines supported earlier by (Chen et al., 2003). It tends to form large circular bodies when it gets enough exposure to red light. The prominent studied model of the possible function of photobodies is that photobodies are a target place for protein degradation (van Buskirk et al., 2012). Primarily PIF3 was found to colocalize with PHYA before its degradation. Moreover, RCD1 was found to interact with PIF3, PIF5, and PIF7 (Jaspers et al., 2009, 2010). One thought might be that RCD1 could either similarly helps in the protein degradation process and further take a role in light signaling events. It would be interesting to study RCD1-PIF colocalization and compare it with PHYB-PIF.

As a highlight of RCD1 interacting with PIFs which mutually interact with PHYB. Our study came to reveal part of this phenomenon. A way to study RCD1 interacting with PHYB was by studying the dynamics of both proteins and their colocalization by Confocal Microscopy. Additionally, using both full length and domain deletion lines to see how each domain could affect the final RCD1 NB colocalization pattern. RCD1ΔRST-3xVenus crossed with *phyB*-5-GFP showed an interesting phenomenon where they showed almost no colocalization with PHYB photobodies, in contrast with other domain deletion lines where they showed partial or complete colocalization. These results suggest the importance of the RST domain and further

complement Vainonen's (2020) results that showed RST domain deleted line enhanced early flowering and tolerance to Methyl viologen; Those considered to be one of the main phenotypes of *rcd1*. In another way, it further validates the importance of RST in RCD1 functioning.

6.2 IDR2 phosphorylation affects RCD1 NB localization

IDRs-containing proteins were more flexible and sensitive to physical-chemical changes in the surrounding. It has known for its accessibility to PTMs as it lacks the tertiary protein structure that helps in their free-moving conformation. PTMs like phosphorylation were found to facilitate LLP separation into MLO (Owen & Shewmaker, 2019) or NB and NB stability (Vainonen et al., 2020). RCD1-IDR2 was a target region for PPKs (Vainonen et al., 2020). IDR2 region in RCD1 was found to affect protein homo or heterodimerization (Wirthmueller et al., 2018); hence, it might be affecting RCD1 protein conformation and scaffolding.

To study the effect of phosphorylation on the IDR2 region, We built Non-phosphorylatable and phosphomimetic forms of RCD1. The development of phosphomutant forms of IDR2 was described earlier (Vainonen et al., 2020). It was essentially done by mutating the residues that are found to be highly phosphorylated by PPKs *in vivo.* In RCD1-$^{S/T}$IDR2^{A}-3xVenus, 15 phosphosites of serine and threonine residues were replaced with non-phosphorylatable alanine. Our results showed that non-phosphorylatable mutation did not affect the subcellular localization of RCD1 NB.Similarly, a non-phosphorylatable MYB gene in *A.thaliana* did not affect protein localization; hence, impaired phosphorylation did not affect subcellular localization (Persak & Pitzschke, 2013).

In the phosphomimetic form of RCD1(RCD1-$^{S/T}$IDR2$^{D/E}$-3xVenus), serine and threonine residues were replaced with aspartic and glutamic amino acids. It showed in some studies using phosphomimetic mutations in a regulatory protein affect both homo and heterodimerization (Gökirmak et al., 2015). Other studies have found that phosphomimetic mutations of HYDROXYPYRUVATE REDUCTASE 1 in *A.thaliana* reduced the photosynthetic CO_2 assimilation rate (Liu et al., 2020). On the contrary, our results have shown that phosphomimetic mutations did not show any localization of RCD1 to NB. This observation may suggest that phosphorylation has negatively affected RCD1 NB localization.

It can be deduced that RCD1 phosphorylation is essential for its stability and localization to NB. In stable lines, It would be worth trying to track T2 plants and measure the RCD1 protein abundance and the percentage of complementation in the *rcd1-4* background.

It has been shown that there is a mutual activity between PIFs and both PHYB (Franklin & Quail, 2010) and RCD1(Jaspers et al., 2009), which points out the role that RCD1 might have in light signalling. Phosphorylation could also be promoted by the interaction of photobodies with transcription regulators, which interestingly brings RCD1, PHYB and phosphorylation into one table. It would be exciting to study the colocalization of phosphomutated RCD1-IDR2 and PHYB-GFP using the RCD1-$^{S/T}$IDR^{A}-3xVenus, RCD1-$^{S/T}$IDR$^{D/E}$-3xVenus, *phyB*-5-GFP

7. Conclusion

This study characterized the RCD1 NB localization pattern using RCD1-3xVenus full length and domain deletion lines complemented in the *rcd1* background. It also revealed that the RST domain showed a colocalization event with *phyB*-5-GFP. Hence, it suggests the importance of the RST domain in protein colocalization and other potential function toward light signaling. Moreover, This study investigated the phosphorylation effect on RCD1 subcellular localization. Non-phosphorylatable and phosphomimetic forms of RCD1- IDR2-3xVenus were used and complemented to *rcd1-4* transient and stable lines. A high abundance of the non-phosphorylatable mutant was detectable, unlike phosphomimetic. Hence, this suggests that phosphorylation of the IDR2 region affects RCD1 protein abundance.

8. References

Bazin, J., Romero, N., Rigo, R., Charon, C., Blein, T., Ariel, F., & Crespi, M. (2018). Nuclear speckle rna binding proteins remodel alternative splicing and the non-coding arabidopsis transcriptome to regulate a cross-talk between auxin and immune responses. *Frontiers in Plant Science*, *9*, 1209. https://doi.org/10.3389/FPLS.2018.01209/BIBTEX

Chen, M., Schwab, R., & Chory, J. (2003). Characterization of the requirements for localization of phytochrome B to nuclear bodies. *Proceedings of the National Academy of Sciences*, *100*(24), 14493–14498. https://doi.org/10.1073/pnas.1935989100

Dundr, M., & Misteli, T. (2010). Biogenesis of Nuclear Bodies. *Cold Spring Harbor Perspectives in Biology*, *2*(12), 711–712. https://doi.org/10.1101/CSHPERSPECT.A000711

Feng, Z., Nagao, H., Li, B., Sotta, N., Shikanai, Y., Yamaguchi, K., Shigenobu, S., Kamiya, T., & Fujiwara, T. (2020). An SMU Splicing Factor Complex Within Nuclear Speckles Contributes to Magnesium Homeostasis in Arabidopsis. *Plant Physiology*, *184*(1), 428–442. https://doi.org/10.1104/PP.20.00109

Franklin, K. A., & Quail, P. H. (2010). Phytochrome functions in Arabidopsis development. *Journal of Experimental Botany*, *61*(1), 11. https://doi.org/10.1093/JXB/ERP304

Gökirmak, T., Denison, F. C., Laughner, B. J., Paul, A. L., & Ferl, R. J. (2015). Phosphomimetic mutation of a conserved serine residue in Arabidopsis thaliana 14-3-3ω suggests a regulatory role of phosphorylation in dimerization and target interactions. *Plant Physiology and Biochemistry*, *97*, 296–303. https://doi.org/10.1016/J.PLAPHY.2015.10.022

Hiltscher, H., Rudnik, R., Shaikhali, J., Heiber, I., Mellenthin, M., Meirelles Duarte, I., Schuster, G., Kahmann, U., & Baier, M. (2014). The radical induced cell death protein 1 (RCD1) supports transcriptional activation of genes for chloroplast antioxidant enzymes. *Front. Plant Sci.*, *5*. https://doi.org/10.3389/fpls.2014.00475

Hyman, A. A., Weber, C. A., & Jülicher, F. (2014). Liquid-Liquid Phase Separation in Biology. *Http://Dx.Doi.Org/10.1146/Annurev-Cellbio-100913-013325*, *30*, 39–58. https://doi.org/10.1146/ANNUREV-CELLBIO-100913-013325

Jády, B., Darzacq, X., Tucker, K. E., Matera, A. G., Bertrand, E., Kiss, T., Ogg, S. C., & Lamond, A. I. (2000). Cajal bodies and coilin-moving towards function. *Annu. Rev. Cell Dev. Biol*, *16*, 17–21.

Jaspers, P., Blomster, T., Brosché, M., Salojärvi, J., Ahlfors, R., Vainonen, J. P., Reddy, R. A., Immink, R., Angenent, G., Turck, F., Overmyer, K., & Kangasjärvi, J. (2009). Unequally redundant RCD1 and SRO1 mediate stress and developmental responses and interact with transcription factors. *Plant Journal*, *60*(2), 268–279. https://doi.org/10.1111/J.1365-313X.2009.03951.X

Jaspers, P., Brosché, M., Overmyer, K., & Kangasjärvi, J. (2010). The transcription factor interacting protein RCD1 contains a novel conserved domain. *Https://Doi.Org/10.4161/Psb.5.1.10293*, *5*(1), 78–80. https://doi.org/10.4161/PSB.5.1.10293

Kalinina, N. O., Makarova, S., Makhotenko, A., Love, A. J., & Taliansky, M. (2018). The multiple functions of the nucleolus in plant development, disease and stress responses. *Frontiers in Plant Science*, *9*, 132. https://doi.org/10.3389/FPLS.2018.00132/BIBTEX

Lafontaine, D. L. J., Riback, J. A., Bascetin, R., & Brangwynne, C. P. (2020). The nucleolus as a multiphase liquid condensate. *Nature Reviews Molecular Cell Biology 2020 22:3*, *22*(3), 165–182. https://doi.org/10.1038/s41580-020-0272-6

Leung, A. K. L. (2014). Poly(ADP-ribose): An organizer of cellular architecture. In *Journal of Cell Biology* (Vol. 205, Issue 5, pp. 613–619). Rockefeller University Press. https://doi.org/10.1083/jcb.201402114

Li, X., Liu, C., Zhao, Z., Ma, D., Zhang, J., Yang, Y., Liu, Y., & Liu, H. (2020). COR27 and COR28 Are Novel Regulators of the COP1-HY5 Regulatory Hub and Photomorphogenesis in Arabidopsis. *The Plant Cell*, *32*(10), 3139–3154. https://doi.org/10.1105/TPC.20.00195

Liu, Y., Guérard, F., Hodges, M., & Jossier, M. (2020). Phosphomimetic T335D Mutation of Hydroxypyruvate Reductase 1 Modifies Cofactor Specificity and Impacts Arabidopsis Growth in Air. *Plant Physiology*, *183*(1), 194–205. https://doi.org/10.1104/PP.19.01225

Love, A. J., Yu, C., Petukhova, N. v., Kalinina, N. O., Chen, J., & Taliansky, M. E. (2017). Cajal bodies and their role in plant stress and disease responses. *RNA Biology*, *14*(6), 779. https://doi.org/10.1080/15476286.2016.1243650

Mach, J. (2016). Phosphorylation and Nuclear Localization of NPR1 in Systemic Acquired Resistance. *The Plant Cell*, *27*(12), 3291–3291. https://doi.org/10.1105/TPC.15.01020

Mao, Y. S., Zhang, B., & Spector, D. L. (2011). Biogenesis and Function of Nuclear Bodies. *Trends in Genetics : TIG*, *27*(8), 295. https://doi.org/10.1016/J.TIG.2011.05.006

Mittelsten Scheid Gregor Mendel-, O. (n.d.). *Crossing of Arabidopsis (for students' lab course manual)*.

Overmyer, K., Tuominen, H., Kettunen, R., Betz, C., Langebartels, C., Sandermann H., J., & Kangasjarvi, J. (2000). Ozone-Sensitive Arabidopsis rcd1 Mutant Reveals Opposite Roles for Ethylene and Jasmonate Signaling Pathways in Regulating Superoxide-Dependent Cell Death. *The Plant Cell*, *12*(10), 1849–1862. https://doi.org/10.1105/TPC.12.10.1849

Owen, I., & Shewmaker, F. (2019). The Role of Post-Translational Modifications in the Phase Transitions of Intrinsically Disordered Proteins. *Int J Mol Sci*, *20*(21), 5501. https://doi.org/10.3390/ijms20215501

Persak, H., & Pitzschke, A. (2013). Tight Interconnection and Multi-Level Control of Arabidopsis MYB44 in MAPK Cascade Signalling. *PLoS ONE*, *8*(2), 57547. https://doi.org/10.1371/JOURNAL.PONE.0057547

Reddy, A. S. N., Day, I. S., Göhring, J., & Barta, A. (2012). Focus Issue on Nuclear Architecture and Dynamics: Localization and Dynamics of Nuclear Speckles in Plants. *Plant Physiology*, *158*(1), 67. https://doi.org/10.1104/PP.111.186700

Santos, A. P., Gaudin, V., Mozgová, I., Pontvianne, F., Schubert, D., Tek, A. L., Dvoøáèková, M., Liu, C., Fransz, P., Rosa, S., & Farrona, S. (2020). Tidying-up the plant nuclear space: Domains, functions, and dynamics. In *Journal of Experimental Botany* (Vol. 71, Issue 17, pp. 5160–5178). Oxford University Press. https://doi.org/10.1093/jxb/eraa282

Shapiguzov, A., Vainonen, J. P., Hunter, K., Tossavainen, H., Tiwari, A., Järvi, S., Hellman, M., Aarabi, F., Alseekh, S., Wybouw, B., Van Der Kelen, K., Nikkanen, L., Krasensky-Wrzaczek, J., Sipari, N., Keinänen, M., Tyystjärvi, E., Rintamäki, E., De Rybel, B., Salojärvi, J., … Kangasjärvi, J. (2019). Arabidopsis RCD1 coordinates chloroplast and mitochondrial functions

through interaction with ANAC transcription factors. *ELife*, *8*, e43284. https://doi.org/10.7554/eLife.43284

Shaw, P. J., & Brown, J. W. (2004). Plant nuclear bodies. *Current Opinion in Plant Biology*, *7*(6), 614–620. https://doi.org/10.1016/J.PBI.2004.09.011

Staněk, D., & Fox, A. (2017). Nuclear bodies: news insights into structure and function. *Current Opinion in Cell Biology*, *46*, 94–101. https://doi.org/10.1016/J.CEB.2017.05.001

Stępiński, D. (2014). Functional ultrastructure of the plant nucleolus. *Protoplasma*, *251*(6), 1285. https://doi.org/10.1007/S00709-014-0648-6

Vainonen, J. P., Jaspers, P., Wrzaczek, M., Lamminmäki, A., Reddy, R. A., Vaahtera, L., Brosché, M., & Kangasjärvi, J. (2012). RCD1-DREB2A interaction in leaf senescence and stress responses in Arabidopsis thaliana. *Biochem J*, *442*(3), 573–581. https://doi.org/10.1042/BJ20111739

Vainonen, J. P., Shapiguzov, A., Krasensky-Wrzaczek, J., Gossens, R., Masi, R. de, Danciu, I., Puukko, T., Battchikova, N., Jonak, C., Wirthmueller, L., Wrzaczek, M., & Kangasjärvi, J. (2020). *Arabidopsis poly(ADP-ribose)-binding protein RCD1 interacts with Photoregulatory Protein Kinases in nuclear bodies*. https://doi.org/10.1101/2020.07.02.184937

van Buskirk, E. K., Decker, P. V., & Chen, M. (2012). Photobodies in Light Signaling. *Plant Physiology*, *158*(1), 52–60. https://doi.org/10.1104/PP.111.186411

Vandereyken, K., van Leene, J., de Coninck, B., & Cammue, B. P. A. (2018). Hub Protein Controversy: Taking a Closer Look at Plant Stress Response Hubs. *Frontiers in Plant Science*, *9*, 694. https://doi.org/10.3389/fpls.2018.00694

Wirthmueller, L., Asai, S., Rallapalli, G., Sklenar, J., Fabro, G., Kim, D. S., Lintermann, R., Jaspers, P., Wrzaczek, M., Kangasjärvi, J., MacLean, D., Menke, F. L. H., Banfield, M. J., & Jones, J. D. G. (2018). Arabidopsis downy mildew effector HaRxL106 suppresses plant immunity by binding to RADICAL-INDUCED CELL DEATH1. *New Phytologist*, *220*(1), 232–248. https://doi.org/10.1111/NPH.15277

Yamaguchi, R., Nakamura, M., Mochizuki, N., Kay, S. A., & Nagatani, A. (1999). Light-dependent translocation of a phytochrome B-GFP fusion protein to the nucleus in transgenic Arabidopsis. *Journal of Cell Biology*, *145*(3), 437–445. https://doi.org/10.1083/jcb.145.3.437

Yang, L., Jiang, Z., Jing, Y., & Lin, R. (2020). PIF1 and RVE1 form a transcriptional feedback loop to control light-mediated seed germination in Arabidopsis. *Journal of Integrative Plant Biology*, *62*(9), 1372–1384. https://doi.org/10.1111/JIPB.12938/SUPPINFO

9. Supplementary data

9.1 Supplementary Table 1. PCR program for *phyB*-5-GFP detection

Cycle name	Temperature (in °C)	Time (in Minutes, seconds)
Initial denaturation	94	1 min
Denaturation	94	10 sec
Primers annealing	58.3	10 sec
Primer extension	72	30 sec
Primer final extension	72	5 min
Cycle x 35		

9.2 Supplementary Table 2. PCR program for RCD1-3xVenus detection

Cycle name	Temperature (in °C)	Time (in Minutes, seconds)
Initial denaturation	94	1 min
Denaturation	94	10 sec
Primers annealing	59	10 sec
Primer extension	72	60 sec
Primer final extension	72	5 min
Cycle x 35		

9.3 Supplementary Table 3. PCR program for RCD1 detection wild type

Cycle name	Temperature (in °C)	Time (in Minutes, seconds)
Initial denaturation	94	1 min
Denaturation	94	10 sec
Primers annealing	55	10 sec
Primer extension	72	1 min 30 sec
Primer final extension	72	5 min
Cycle x 35		

9.4 Supplementary Table 4. PCR program for *rcd1-4* detection T-DNA insertion

Cycle name	Temperature (in °C)	Time (in Minutes, seconds)
Initial denaturation	94	1 min
Denaturation	94	10 sec
Primers annealing	52	10 sec
Primer extension	72	30 sec
Primer final extension	72	5 min
Cycle x 35		

9.5 Supplementary Table 5. PCR program for *phyB-5* detection

Cycle name	Temperature (in °C)	Time (in Minutes, seconds)
Initial denaturation	94	1 min
Denaturation	94	10 sec
Primers annealing	63	10 sec
Primer extension	72	10 sec
Primer final extension	72	5 min
Cycle x35		

9.6 Supplementary Table 6. Insert and backbone amplification reaction mixture

Components	quantity (ul) tot. vol. =50ul	Scalable quantity (2.2X)	3.2X	4.2X	5.2X	6.2X	7.2X	8.2X	9.2X	10.2X
dNTPs	1	2.2	3.2	4.2	5.2	6.2	7.2	8.2	9.2	10.2
Forward Primer	1	2.2	3.2	4.2	5.2	6.2	7.2	8.2	9.2	10.2
Reverse Primer	1	2.2	3.2	4.2	5.2	6.2	7.2	8.2	9.2	10.2
5x HF buffer	5	11	16	21	26	31	36	41	46	51
Phusion DNA polymerase	0.5	1.1	1.6	2.1	2.6	3.1	3.6	4.1	4.6	5.1
MQ water	40.5	89.1	129.6	170.1	210.6	251.1	291.6	332.1	372.6	413.1
Total Volume	49									

9.7 Supplementary Table 7. PCR programme for RCD1-IDR2 insert amplification

Cycle name	Temperature (in °C)	Time (in Minutes, seconds)
Initial denaturation	98	30 sec
Denaturation	98	10 sec
Primers annealing	71	10 sec
Primer extension	72	33 sec
Primer final extension	72	5 min
Cycle x35		

9.8 Supplementary Table 8. PCR programme for pDONR-RCD1 backbone amplification

Cycle name	Temperature (in °C)	Time (in Minutes, seconds)
Initial denaturation	98	30 sec
Denaturation	98	10 sec
Primers annealing	57	10 sec
Primer extension	72	6 min 15 sec
Primer final extension	72	5 min
Cycle x 35		

9.9 Supplementary Table 9. Golden gate cloning reaction mixture

Cloning mix	1 reaction (ul)	2 reaction (2.2X)	4 reactions
10x Buffer G	1.5	3.3	6.3
10mM ATP	0.75	1.65	3.15
100x BSA (Bovine Serum Albumine)	0.15	0.33	0.63
T4 DNA Ligase	1	2.2	4.2
BsaI (Eco31I)	1	2.2	4.2
dH_2O	1.55	3.41	6.51
Intermediate volume	5		

9.10 Supplementary Table 10. Multisite Gateway cloning LR reaction mixture

Reaction components	Volume (µl)/ reaction
Entry Clones (10 fmoles)	1-7
Destination vector (20 fmoles)	1
1X TE buffer, pH 8.0	Fill up to 8
LR Clonase^{TM}II Plus Enzyme Mix	2
Proteinase K	1

9.11 Supplementary Table 11. Restriction digestion reaction

Reaction components	Volume (µl)/ reaction
DNA (1 µg)	1
10X FD buffer	2
pstI FD enzyme	1
MQ water	Up to 20

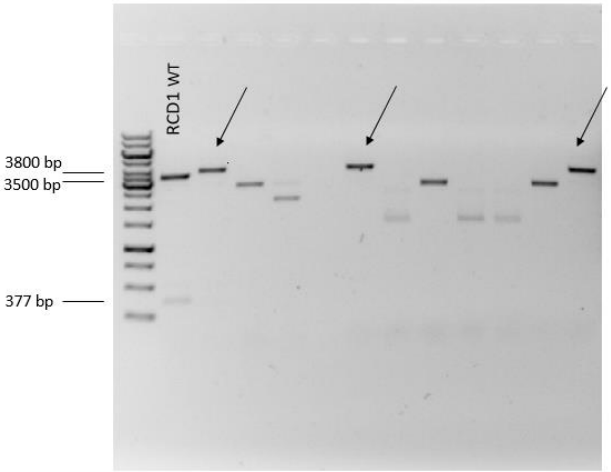

Supplementary Figure 1. *pstI* digestion for RCD1 golden gate clones. Arrows points the positive clones.pDONR-RCD1 used as negative control for non- phosphorylatable PDONR-RCD1-STIDR2^{A}

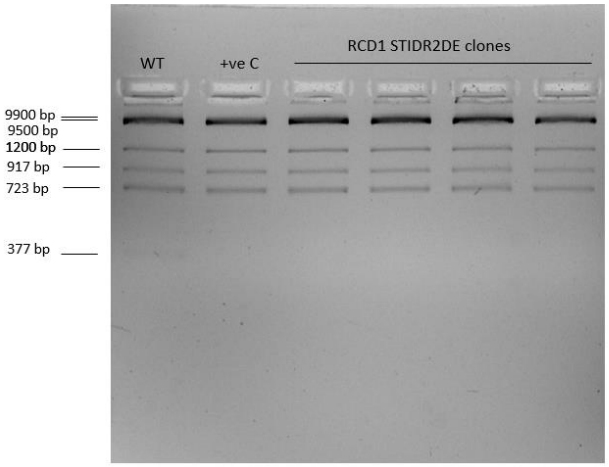

Supplementary Figure 2. *pstI* digestion for RCD1 multisite gateway clones WT;wild type, pBm43GW-pUBQ-RCD1-3xVenus , +ve C(positive control); pBm43GW-pUBQ-RCD1-STIDR2A-3xVenus, pBm43GW-pUBQ-RCD1-STIDR2DE-3xVenus.

9.12 Supplementary Code 1.

```
var list = getList("image.titles");
var path = getInfo("image.directory");
print(path);
for (i=0; i<list.length; i++){
	print("Current series:   " + list[i]);
	// Condense z-stack & polish image
	selectWindow(list[i]);
	run("Z Project...", "projection=[Max Intensity]");
	run("Stack to Images");
	var title = getTitle();
	print("Current title:   " + title);
	for (j=1; j<5; j++){
		selectWindow(replace(title, "-0004", "-000" + j));
		run("Gaussian Blur...", "sigma=2");
		setMinAndMax(1, 255);

		//Reassign colour
		// 0001   Green		PhyB-GFP
		// 0002   Magenta		ChlAF
		// 0003   Red		RCD1-3xVenus
		// 0004   Gray		Brightfield
		colour = newArray("", "Green", "Magenta", "Red", "Grays");
		run(colour[j]);

		print("Save:" + path + replace(replace(replace(list[i], ".lif - ", ""), "/", "-"), " ", "_") + "-000" +
j);
		saveAs("TIFF" , path + replace(replace(replace(list[i], ".lif - ", ""), "/", "-"), " ", "_") + "-000" +
j);
	}
	//Create merge image
	title = getTitle();
	print(title);
	//Merge channels
	//C1 - Red
```

```
//C2 - Green

//C3 - Blue

//C4 - Gray

//C5 - Cyan

//C6 - Magenta

//C7 - Yellow

run("Merge Channels...", "c1=" + replace(title, "0004", "0003") + " c2=" + replace(title, "0004", "0001")
+ " create keep");


// Set scale bar (1 µm)

run("Scale Bar...", "width=1 height=4 font=14 color=White background=None location=[Lower Right]
bold overlay");

saveAs("TIFF", path + replace(title, "0004", "merge-RFP-Venus"));

close();

run("Merge Channels...", "c1=" + replace(title, "0004", "0003") + " c2=" + replace(title, "0004", "0001")
+ " c6=" + replace(title, "0004", "0002") + " create keep");

// Set scale bar (1 µm)

run("Scale Bar...", "width=1 height=4 font=14 color=White background=None location=[Lower Right]
bold overlay");

saveAs("TIFF", path + replace(title, "0004", "merge-RFP-Venus-ChlAF"));

close();

run("Merge Channels...", "c1=" + replace(title, "0004", "0003") + " c2=" + replace(title, "0004", "0001")
+ " c4=" + replace(title, "0004", "0004") + " create keep");

// Set scale bar (1 µm)

run("Scale Bar...", "width=1 height=4 font=14 color=White background=None location=[Lower Right]
bold overlay");

saveAs("TIFF", path + replace(title, "0004", "merge-RFP-Venus-BF"));

close();

run("Merge Channels...", "c1=" + replace(title, "0004", "0003") + " c2=" + replace(title, "0004", "0001")
+

" c4=" + replace(title, "0004", "0004") + " c6=" + replace(title, "0004", "0002") + " create keep");

// Set scale bar (1 µm)

run("Scale Bar...", "width=1 height=4 font=14 color=White background=None location=[Lower Right]
bold overlay");

saveAs("TIFF", path + replace(title, "0004", "merge-all"));

close();

close(title);

close(replace(title, "4", "1"));

close(replace(title, "4", "2"));
```

```
	close(replace(title, "4", "3"));
	close(list[i]);

	if (i+1==list.length){
		print("All series in LIF file have been processed");
	} else {
		selectWindow(list[i+1]);
	}
}
```

9.13 Supplementary Code 2.

```
var list = getList("image.titles");
var path = getInfo("image.directory");
print(path);

for (i=0; i<list.length; i++)}
	print("Current series:   " + list[i]);

	 //Condense z-stack & polish image
	selectWindow(list[i]);
	run("Z Project...", "projection=[Max Intensity]");
	run("Stack to Images");
	var title = getTitle;()
	print("Current title:   " + title);

	for (j=1; j<4; j++)}
		selectWindow(replace(title, "-0003", "-000" + j));
		run("Gaussian Blur...", "sigma=2");
		setMinAndMax;(255 ,1)

		//Reassign colour
		 0001 // Red			RCD1-3xVenus
		 0002 // Magenta		ChlAF
```

```
0003 // Gray                    Brightfield
colour = newArray("", "Red", "Magenta", "Grays");
run(colour[j]);


//Set scale bar (1 µm)
run("Scale Bar...", "width=1 height=4 font=14 color=White background=None location=[Lower Right] bold overlay");
print("Save:" + path + replace(replace(replace(list[i], ".lif - ", ""), "/", "-"), " ", "_") + "-000" + j);
saveAs("TIFF" , path + replace(replace(replace(list[i], ".lif - ", ""), "/", "-"), " ", "_") + "-000" + j);
{
//Create merge image
title = getTitle;()
print(title);
//Merge channels
//C1 - Red
//C2 - Green
//C3 - Blue
//C4 - Gray
//C5 - Cyan
//C6 - Magenta
//C7 - Yellow


run("Merge Channels...", "c1=" + replace(title, "0003", "0001") + " c4=" + replace(title, "0003", "0003") + " create keep");
//Set scale bar (1 µm)
run("Scale Bar...", "width=1 height=4 font=14 color=White background=None location=[Lower Right] bold overlay");
saveAs("TIFF", path + replace(title, "0003", "merge-Venus-BF"));
close;()
run("Merge Channels...", "c1=" + replace(title, "0003", "0001") + " c6=" + replace(title, "0003", "0002") + " create keep");
//Set scale bar (1 µm)
```

```
        run("Scale Bar...", "width=1 height=4 font=14 color=White background=None
location=[Lower Right] bold overlay");

        saveAs("TIFF", path + replace(title, "0003", "merge-Venus-chlAF"));

        close;()

        run("Merge Channels...", "c1=" + replace(title, "0003", "0001") + " c6=" + replace(title,
"0003", "0002") + " c4=" + replace(title, "0003", "0003") + " create keep");

         //Set scale bar (1 µm)

        run("Scale Bar...", "width=1 height=4 font=14 color=White background=None
location=[Lower Right] bold overlay");

        saveAs("TIFF", path + replace(title, "0003", "merge-all"));

        close;()


        close(title);

        close(replace(title, "3", "1"));

        close(replace(title, "3", "2"));

        close(list[i]);


        if (i+1==list.length)}

                print("All series in LIF file have been processed");

         {else}

                selectWindow(list[i+1]);

        {
{
```